NASA MEMO 6-4-59L

NASA

MEMORANDUM

DISTRIBUTION OF HEAT TRANSFER ON A 10° CONE AT ANGLES OF ATTACK FROM 0° TO 15° FOR MACH NUMBERS OF 2.49 TO 4.65 AND A SOLUTION TO THE HEAT-TRANSFER EQUATION THAT PERMITS COMPLETE MACHINE CALCULATIONS

By Paige B. Burbank and B. Leon Hodge

Langley Research Center
Langley Field, Va.

NATIONAL AERONAUTICS AND SPACE ADMINISTRATION

WASHINGTON

June 1959

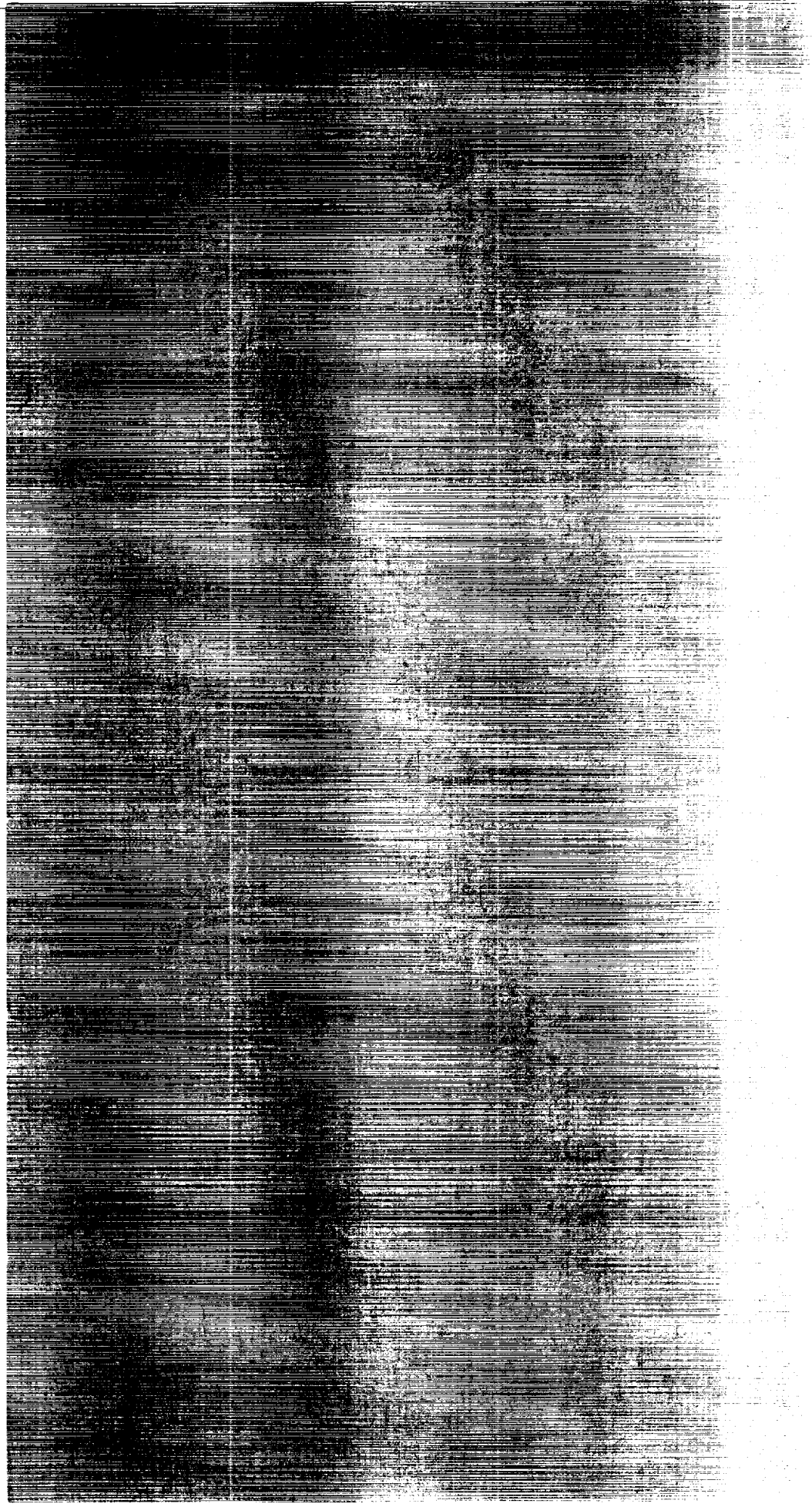

NATIONAL AERONAUTICS AND SPACE ADMINISTRATION

MEMORANDUM 6-4-59L

DISTRIBUTION OF HEAT TRANSFER ON A 10° CONE AT ANGLES OF ATTACK FROM 0° TO 15° FOR MACH NUMBERS OF 2.49 TO 4.65 AND A SOLUTION TO THE HEAT-TRANSFER EQUATION THAT PERMITS COMPLETE MACHINE CALCULATIONS

By Paige B. Burbank and B. Leon Hodge

SUMMARY

The pressure and heat-transfer distribution were measured on the surface of a thin-walled 10° cone for a Mach number range from 2.49 to 4.65 at angles of attack from 0° to 15° in the Langley Unitary Plan wind tunnel. The results indicate that Kopal's theory adequately predicts the surface Mach number for heat-transfer calculations.

The measured laminar heat-transfer coefficients at an angle of attack of 0° are in good agreement with Van Driest theory having a Mangler transformation. At angle of attack the heat-transfer coefficient along the stagnation line is 1.9 to 4 times greater than at an angle of attack of 0° depending upon the distance from the tip of the nose, Reynolds number, and Mach number. Boundary-layer transition and body vortices caused minimum heat-transfer coefficients to occur at the 90° and 120° meridian angles and increased aerodynamic heating along the 180° meridian that in some cases is of the same magnitude as that along the zero meridian (stagnation line). A method was developed for complete machine calculation of the heat-transfer coefficient from transient temperature measurements.

INTRODUCTION

Aerodynamic heating is one of the primary factors to be considered in the design of aerodynamic or ballistic missiles operating at high velocity within the earth's atmosphere. The large heat-transfer coefficients that occur in the stagnation regions of supersonic vehicles has created a great deal of concern as to the magnitude of increase of heat-transfer coefficients along the windward surface of bodies at angles of attack. The purpose of this investigation is to determine the effect of angle of attack on the magnitude and distribution of heat-transfer

coefficients on a 10° cone. The distribution of heat-transfer coefficients at an angle of attack of 0° that is readily predictable from flat-plate theory and the use of the Mangler transformation was also measured and compared with the theoretical values presented in reference 1.

The transitional Reynolds number on a 10° cone has been used as a comparison of the steadiness of the flow in several facilities. (See ref. 2.) In this investigation the transition Reynolds number was also determined from equilibrium temperature measurements on the 10° cone at five Mach numbers from 2.49 to 4.65 in the high Mach number test section of the Langley Unitary Plan wind tunnel.

The heat-transfer coefficients were determined from transient skin temperature measurements resulting from a stepwise increase in the stagnation temperature. This method necessitates the evaluation of the slope of the temperature-time history. Graphical solution of the slope is time consuming for models incorporating many thermocouples and inaccurate in regions of low heat transfer. Consequently, the basic heat-transfer equation was rewritten in an integral form that permits complete machine calculation and increases the accuracy in regions of low heat transfer. The details of this integral solution and a comparison with a machine-slope solution are discussed in the appendix. A new method of recording the thermocouple output that converts the electrical input into digital form was used to eliminate the use of recording oscillographs or self-balancing potentiometers.

SYMBOLS

A, C	constants
c	specific heat of skin material, Btu/lb-$^{\circ}$R
c_p	specific heat of air at constant pressure, Btu/lb-$^{\circ}$R
g	acceleration due to gravity, ft/sec^2
h	heat-transfer coefficient, Btu/ft^2-sec-$^{\circ}$R
h_{av}	arithmetic average heat-transfer coefficient, Btu/ft^2-sec-$^{\circ}$R
Δh	deviation in h defined in equation (3)
k	arbitrary constant in equation (A7)

l	length of model, 2.15 feet
M	Mach number
R	Reynolds number per foot, $\rho V/\mu$
N_{St}	Stanton number, $h_{av}/\rho V c_p g$
t	time, sec
Δt	denotes time increment between temperature measurements
T	temperature, ^{o}R
T_e	effective stream air temperature at wall, some temperature which gives a thermal potential that is independent of heat-transfer coefficient, ^{o}R
T_w	wall temperature, ^{o}R
T_t	stagnation temperature, ^{o}R
V	velocity, ft/sec
w	specific weight of skin material, lb/sq ft
x	longitudinal distance along model, ft
α	angle of attack, deg
η_r	recovery factor defined in equation (4)
ϕ	meridian angle, deg
ρ	free-stream density of air, slugs/cu ft
μ	dynamic viscosity coefficient, lb-sec/sq ft
$\chi = T_e/T_t$	(See eq. (A4))

Subscripts and superscripts:

s	surface
tr	transition

∞	free stream
0,1,2,3,. . . n	time sequence
max	maximum
min	minimum

A prime over a symbol denotes smooth values.

MODEL DESCRIPTION

The thin-walled 10° cone used in these tests is illustrated in figure 1. The model was constructed by spinning a 0.030-inch Inconel sheet on a mandril. The nose was machined from solid Inconel to a uniform thickness of 0.030 inch to within $1\frac{3}{8}$ inches of the conical apex and was Inconel-welded to the spun portion of the body. The model was instrumented with 47 iron-constantan thermocouples and 4 static-pressure orifices; the locations of the thermocouples and the pressure orifices are shown in figure 2 and the local skin thicknesses are listed in table I. Thermocouples 1 to 5 were inoperative during this investigation. Special care was taken, as shown in the thermocouple detail in figure 2, to assure that the thermocouple junction was in the model skin. The main portion of the model was instrumented with No. 36 gage wire; however, at $x/l = 0.24$, 0.48, 0.71, and 0.86, three wire sizes (No. 24, 30, and 36 gage) were installed every 30° about the body from $\phi = 0^{\circ}$ to $\phi = 180^{\circ}$ to determine the effect of wire size on the temperature-time history during a stepwise increase in stagnation temperature. The temperature-time histories obtained at an angle of attack of 0° indicated no significant difference in the temperature response for the wire sizes tested. The base of the model was sealed with a 1/2-inch disk of paraplex and the interior of the model was vented to free-stream static pressure to minimize internal heat convection. The model surface was polished by the process outlined in appendix B of reference 3 to a finish of $1\frac{1}{2}$ microinches root mean square as determined by a profilometer. The stagnation temperature was determined by a probe mounted in the plane of the base of the instrumented cone as shown in figure 1.

APPARATUS

The thermocouple output was recorded with a Consolidated Engineering Corporation Millisadic System - a multichannel sequential analog to

digital conversion system. The principal advantage of this system is that it converts the thermocouple output into digital form almost at the same time the test is being conducted. It can sample in sequence 100 analog inputs at the rate of 4 times a second and convert the inputs into digital form and record the values on a magnetic tape which, in turn, is fed into a card-punch machine for tabulation. This system, illustrated in the block diagram of figure 3, is composed of a voltage pickup, an amplifier, a relay switch, a voltage to digital converter, and a tape recorder. The full scale of 1,000 counts can represent 5 or 10 millivolts. The resolution of one count gives an accuracy of $1/3^{\circ}$ R for the 10-millivolt range when iron-constantan thermocouples are used.

The static pressures were measured with electrical transducers having an accuracy of 10 pounds per square foot.

The tests were conducted in the high Mach number test section of the Langley Unitary Plan wind tunnel. The variation of the free-stream Mach number in the vicinity of the model is presented in the following table:

M	ΔM
2.49	±0.01
2.98	±.01
3.51	±.04
3.96	±.05
4.65	±.04

METHOD OF DATA REDUCTION

Transient temperature measurements on a thin-walled model that result from a stepwise increase in the stagnation temperature can be used to determine the heat-transfer coefficient from the following relation that omits the conduction and radiation terms:

$$h = \frac{wc\left(dT_w/dt\right)}{T_e - T_w} \tag{1}$$

A typical temperature-time history for a stagnation-probe thermocouple and a wall thermocouple on the 10° cone during a heat burst is illustrated in figure 4(a) for a Mach number of 2.49 and in figure 4(b) for a Mach number of 3.96.

In order to eliminate the determination of the slope of the temperature-time curve, the general heat-transfer equation was rewritten in an integral form and the heat-transfer coefficient was determined from the following relation:

$$h = \frac{wc\left(T_{w,n} - T_{w,0}\right)}{\frac{T_e}{T_0}\sum_{0}^{n} T_t - \sum_{0}^{n} T_w} \qquad (2)$$

and the summations were evaluated by using the trapezoidal rule.

The development of this equation and a comparison of the integral, a machine-computed slope, and graphical-slope methods for determining heat-transfer coefficients are presented in the appendix.

TEST PROCEDURE

The procedure for a typical heat-transfer test was to reduce the stagnation temperature to approximately 140° F and to monitor one of the thermocouples (in this case thermocouple 42 on the cone) on a self-balancing potentiometer. When this thermocouple had indicated that equilibrium had been attained, a scan of all thermocouples was made to determine $\left(T_e/T_t\right)_1$. Then the stagnation temperature was given a stepwise increase, the coolers in the tunnel circuit being bypassed during which time the thermocouple output was continuously recorded at 1/2-second intervals for 1 minute. The stagnation temperature was held at an elevated level for an additional 4 minutes at which time another scan of the thermocouple was made to determine $\left(T_e/T_t\right)_2$. A comparison of the $\left(T_e/T_t\right)_1$ and $\left(T_e/T_t\right)_2$ indicated that the ratios agreed within the experimental accuracy and that the type of boundary layer on the model was unaffected by the stepwise increase in the stagnation temperature utilized in these tests.

The beginning time for integration of equation (2) was the earliest time that the stagnation temperature probe, located at the base of the model, had reached the elevated level. The random oscillations in the stagnation temperature during the 25-second time interval used for heat-transfer calculations, was less than 4 percent of the average stagnation temperature.

RESULTS AND DISCUSSION

Pressure Measurements

The results of the static-pressure measurements at two meridian angles (0° and 180°) and two axial stations are shown in figure 5. The results of the high Reynolds number pressure measurements at four points on the 10° cone at an angle of attack of 0° are in good agreement with Kopal's theory (refs. 4, 5, and 6) as shown in figure 5(a). The scatter that occurs at the higher Mach numbers is within the accuracy of the pressure measurements. In figures 5(b) and 5(c), the measured surface Mach number for α of 7.5° and 15° is compared with theory for $\phi = 0^\circ$ and 180°. At both angles of attack Kopal's theory adequately predicts the surface Mach number for heat-transfer calculations, although the calculated values are somewhat lower than the measured values at $\phi = 180^\circ$ and $\alpha = 15^\circ$.

Heat-Transfer Tests

The heat-transfer coefficient h computed from equation (2) was listed for every 2 seconds throughout the time of integration as shown in table II. All integrations are taken from the time zero to the time listed. The combined effect of the difference between adiabatic and equilibrium temperature ratios and the influence of conduction on the wall temperature results in a small variation of h with time. Therefore, the results are presented as the dimensionless Stanton number based on free-stream conditions and using the arithmetic average of the heat-transfer coefficients.

In figure 6 the Stanton number distribution on the 10° cone at an angle of attack of 0° is compared with the laminar theory of reference 1. The deviation of the heat-transfer coefficient over the total time of integration is also shown in figure 6 where the deviation Δh is defined in percent as

$$\Delta h = \frac{h_{max} - h_{min}}{2} \frac{100}{h_{av}} \tag{3}$$

With the exception of that portion of the model affected by boundary-layer transition, the agreement of the experimental data with the Van Driest theoretical heat-transfer coefficient modified by the Mangler transformation is very good.

The boundary-layer transition occurred for all test conditions except for $M = 2.49$ at $R = 1.68 \times 10^6$ and $M = 2.98$ at

$R = 1.80 \times 10^6$. At $M = 3.51$ at $R = 1.88 \times 10^6$ and $M = 3.96$ at $R = 1.99 \times 10^6$ transition occurred at $x/l > 0.7$. At the higher Reynolds numbers transition occurred at x/l of about 0.5 for all Mach numbers. It is to be noted that, when transition does occur, the variation of h with meridian angle indicates that the position of transition varies about the body.

The effect of angle of attack on the distribution of the heat-transfer coefficient is shown in figures 7 and 8. The axial distribution along the zero meridian line as shown in figure 7 illustrates the increase of heat-transfer coefficient with angle of attack. The magnitude of the increase can be expressed as the ratio, at a particular thermocouple, of the Stanton number at an angle of attack to the Stanton number at an angle of attack of 0° $\frac{N_{St,\alpha}}{N_{St,\alpha=0}}$. The magnitude of the ratio varies from approximately 1.9 to 4 and depends upon the distance from the tip of the nose, the free-stream Reynolds number, and the Mach number as shown in the following table:

Mach number, M	$\alpha = 7.5^\circ$		$\alpha = 15^\circ$	
	$R = 1.68 \times 10^6$ to 2.30×10^6	$R = 3.36 \times 10^6$ to 4.10×10^6	$R = 1.68 \times 10^6$ to 2.30×10^6	$R = 3.36 \times 10^6$ to 4.10×10^6
$x/l = 0.28$				
2.49	2.24	1.87	2.61	3.28
2.98	2.36	2.07	3.28	3.13
3.51	2.29	2.27	3.15	3.36
3.96	2.41	2.35	3.37	3.71
4.65	----	----	3.45	----
$x/l = 0.55$				
2.49	2.24	0.85	2.96	1.52
2.98	2.53	.51	3.53	.81
3.51	2.81	.50	4.02	.76
3.96	2.69	.74	4.02	1.16
4.65	----	----	3.73	----

The Reynolds number varies slightly with each step increase in stagnation temperature; therefore the Reynolds numbers for figure 7 and table III are average values. The laminar-flow heat-transfer ratio

tends to increase with Mach number and the magnitude of the increase becomes greater, as the angle of attack is increased.

Along the afterportion of the cone the ratio $\frac{N_{St,\alpha}}{N_{St,\alpha=0}}$ is a ratio of laminar to turbulent heat-transfer coefficients at the higher Reynolds number. The boundary transition at x/l of approximately 0.5 at $\alpha = 0^\circ$ results in a low transitional Reynolds number. However, at angles of attack the crossflow introduces a favorable circumferential pressure gradient that reduces the boundary layer along the stagnation line and increases the stability of the laminar flow. Consequently, the high turbulent heat-transfer coefficients that occurred along the afterportion of the body for some of the test conditions at $\alpha = 0$, as shown in figure 7, do not occur on the stagnation line at an angle of attack. This results in some values of $\frac{N_{St,\alpha}}{N_{St,\alpha=0}}$ less than 1 for $x/l = 0.55$ as shown in the preceding table.

Variation of the N_{St} with ϕ at $R = 1.7 \times 10^6$.- The effect of angle of attack on the distribution of the Stanton number about the body at four axial stations is shown in figure 8 for $M_\infty = 2.49$. At the foremost axial station ($x/l = 0.24$) shown in figure 8(a) the Stanton number is constant with ϕ for zero angle of attack. At an angle of attack the heat-transfer coefficient increases along the stagnation line and decreases with increasing ϕ to a minimum at $\phi = 120^\circ$. Turbulent flow and body vortices along the leeward portion of the cylinder cause N_{St} to increase for ϕ greater than 120°. At α of 7.5° the Stanton number is greater at $\phi = 180^\circ$ than at $\phi = 0^\circ$. As the angle of attack is increased to 15°, the value of N_{St} also increases on the lee side; however, the increase in N_{St} is less for a change in α from 7.5° to 15° than for a change from 0° to 7.5°. At $\alpha = 15^\circ$ the Stanton number is approximately of the same magnitude for ϕ of 0° and 180°. The same variation of Stanton number with ϕ for the angle-of-attack range appears at the three other axial stations as shown in figures 8(b) to 8(d), with the exception of the data obtained at ϕ of 150° and 180° for $x/l = 0.48$ and 0.71. At these two meridian angles $N_{St,\alpha}$ reaches a maximum at $\alpha = 7.5^\circ$ and decreases at $\alpha = 15^\circ$. The agreement of four thermocouples at both axial stations tends to minimize the possibility of faulty data. At the $x/l = 0.71$ the minimum heat transfer occurs at $\phi = 90^\circ$. At $x/l = 0.86$, data were obtained only for the thermocouples from ϕ of 0° to 90°.

The effect of increasing the Reynolds number on the N_{St} distribution.- The effect of increasing the Reynolds number by a factor

of about two is also shown in figure 8. At the foremost axial station the overall distribution of Stanton number with ϕ is similar to the low Reynolds number data; however, the increase of N_{St} with α is uniform over the entire α range. As the distance along the body is increased, the effect of varying degrees of turbulence in the boundary layer about the body gives Stanton number fluctuations from laminar to full turbulent values.

In table III the ratio $\frac{N_{St,\alpha}}{N_{St,\alpha=0}}$ is given for $\phi = 0^\circ$, 120°, and 180° for all Mach numbers and Reynolds numbers.

Transitional Reynolds Number

The transitional Reynolds number was determined from the local recovery factor computed from equilibrium temperature measurements of the thermocouples located on a conical ray in the zero meridian plane. The recovery factor was computed from the following relation:

$$\eta_r = \frac{\frac{T_e}{T_t} - \frac{T_\infty}{T_t}}{1 - \frac{T_\infty}{T_t}} \qquad (4)$$

where the free-stream conditions were for the local Mach number just outside the boundary layer determined from reference 4. The resultant variations of η_r with x/l for $M_\infty = 2.49$ to $M_\infty = 4.65$ are shown in figure 9. The surface lengths corresponding to the flagged points were used to determine the transitional Reynolds number. For free-stream Reynolds numbers of 2.0×10^6 to 2.6×10^6 per foot, the transitional Reynolds numbers varied from 2.4×10^6 to 3.1×10^6. A comparison (fig. 10) of the transitional Reynolds numbers determined in the Langley Unitary Plan wind tunnel with the results of reference 2 indicated that the wind tunnel has relatively smooth flow in spite of a complicated ducting leading to the test section and an asymmetric nozzle used to develop supersonic flow.

CONCLUDING REMARKS

The results indicate that existing theory for calculating surface Mach number is in excellent agreement with measured values for angles

of attack of 0° and 7.5°. At an angle of attack of 15° the deviation between theoretical and measured surface Mach number is negligible for heat-transfer calculations.

The measured laminar heat-transfer coefficients at an angle of attack of 0° are in good agreement with Van Driest theory having a Mangler transformation. At angle of attack the heat-transfer coefficient along the stagnation line is 1.9 to 4 times greater than at zero angle of attack depending upon x/l, Reynolds number, and Mach number. Boundary-layer transition and body vortices cause minimum heat-transfer coefficients to occur at the 90° and 120° meridian angles and increased aerodynamic heating along the 180° meridian that, in some cases, is of the same magnitude as along the stagnation line.

Langley Research Center,
National Aeronautics and Space Administration,
Langley Field, Va., March 17, 1959.

APPENDIX

DEVELOPMENT OF A SOLUTION TO THE HEAT-TRANSFER EQUATION THAT PERMITS COMPLETE MACHINE CALCULATION

The heat-transfer coefficient can be determined from transient temperature measurements, resulting from a stepwise increase in T_t, from the following relation which assumes constant temperature through the skin, negligible lateral heat flow, negligible heat flow to the backup material, and no losses due to radiation:

$$h = \frac{wc \frac{dT_w}{dt}}{T_e - T_w}$$

The slope of the wall-temperature variation with time $\frac{dT_w}{dt}$ can be obtained graphically; however, for a heat-transfer test incorporating many thermocouples, plotting and fairing the curves for each test point is very time consuming and necessitates a method of machine calculation. An alternate method of determining the slope of the wall-temperature curve is readily adaptable to machine calculations. This method outlined in appendix B of reference 7 fairs the temperature-time curve by taking five successive measured points in time and determines a faired value of the midpoint by use of a binomial filter as in the following equation:

$$T_3' = \frac{1T_1 + 4T_2 + 6T_3 + 4T_4 + 1T_5}{16} \tag{A1}$$

A cubic was fitted to the faired temperatures and the slope was determined from the following relation:

$$\left(\frac{dT}{dt}\right)_3 = \frac{1T_1' - 8T_2' + 0T_3' + 8T_4' - 1T_5'}{12(\Delta t)} \tag{A2}$$

(where the subscripts denote the time sequence). The preceding solution, as will be shown later, does not adequately fair the oscillations encountered in the stagnation temperature; therefore the following solution was developed.

In order to eliminate the determination of the slope of the temperature-time curve, the general heat-transfer equation was written in the following form:

$$\chi \int_0^t T_t \, dt - \int_0^t T_w \, dt = \frac{wc}{h} \int_{T_{t=0}}^{T_{t=t}} dT_w \tag{A3}$$

where

$$\chi = \frac{T_e}{T_t} = \frac{1 + \frac{\gamma - 1}{2} \eta_r M^2}{1 + \frac{\gamma - 1}{2} M^2} \tag{A4}$$

Then, replacing the integrals with summations yields

$$h = \frac{wc\left(T_{w,n} - T_{w,0}\right)}{\chi \sum_0^n T_t - \sum_0^n T_w} \tag{A5}$$

where

$$\sum_0^n T = \Delta t\left(\frac{1}{2} T_0 + \frac{1}{2} T_n + T_1 + T_2 + T_{n-1}\right) \tag{A6}$$

In order to determine the accuracy of the integral solution of equation (A5), the method was applied to the following conditions: A typical wall temperature-time history was represented by an exponential of the form

$$T = A\left(1 - e^{-kt}\right) + C \tag{A7}$$

With a constant stagnation temperature and the product of $wc = 1$ and an assumed nominal value of a recovery factor, the value of h was 0.0636 and independent of the time. The integral and the slope method gave the same results, but the slope method had an increasing scatter in h as the slope of the wall temperature-time curve approached zero.

The ability of the integral solution to determine the heat-transfer coefficient when errors occurred in the wall and stagnation temperature-time histories was demonstrated by superimposing random errors (of a

magnitude determined from preliminary experimental measurements) on the smooth temperature-time histories. In one case the wall temperature was represented by the true exponential; a Gaussian distribution of temperature errors with a root mean square of 3° was superimposed on the stagnation temperature. This procedure would result in 99 percent of the stagnation temperatures having a deviation of less than 9°. The results illustrated in figure 11(a) indicate the integral solution is within 4 percent of the actual value 0.0636. It should be pointed out that the stagnation temperature-time curve shown in figure 4 does not indicate random errors but actually a low-frequency oscillation which would tend to reduce the scatter indicated in figure 11.

With the stagnation temperature held constant, the wall temperature had a random error with a root mean square of 0.6° superimposed on the true exponential. If the same percentage of area is taken under the bell curve, a maximum error of 1.8° would be obtained, and the results in figure 11(b) are within ± 3 percent of 0.0636.

The powerful smoothing action of the integral solution is shown in figure 11(c), which illustrates the effect of random errors in both wall and stagnation temperature; the data are within 4 percent of the true value. The inability of the machine-computed slope method, utilizing equations (A1) and (A2), to handle random errors in the temperature-time histories is illustrated in figure 12. Decreasing dT_w/dt radically increases the scatter in h.

In a preliminary test on the 10° cone, the heat-transfer coefficient was determined at $x/l = 0.07$ and 0.32 by the graphical slope, machine-computed slope method utilizing equations (A1) and (A2) and the integral solution. The variation of h with t for the graphical slope and the integral solution for $x/l = 0.07$ is shown in figure 13(a). The limits of integration were fixed to omit the initial curvature of the stagnation temperature during the temperature bump. The graphical solution using faired T_w and T_t values would be accurate in the earlier times because of the steeper slopes and the integral solution more accurate at later times where the area of integration becomes large. In figure 13(b), the same comparison is made for $x/l = 0.32$. The integral solution agrees well with the value obtained by the graphical solution. The results of the machine-slope method for $x/l = 0.07$ are compared with the graphical method in figure 13(c). The large scatter of ± 20 percent indicates the need for a much more powerful fairing method than that represented by equations (A1) and (A2).

In conclusion the integral solution is an accurate method for complete machine calculation of the heat-transfer coefficients.

REFERENCES

1. Van Driest, E. R.: The Problem of Aerodynamic Heating. Aero. Eng. Rev., vol. 15, no. 10, Oct. 1956, pp. 26-41.

2. Ross, Albert O.: Determination of Boundary-Layer Transition Reynolds Numbers by Surface-Temperature Measurement of a 10° Cone in Various NACA Supersonic Wind Tunnels. NACA TN 3020, 1953.

3. Burbank, Paige B.: A Method for Calculating the Contour of Bodies of Revolution With a Prescribed Pressure Gradient at Supersonic Speed With Experimental Verification. NACA TN 3555, 1956.

4. Staff of the Computing Section, Center of Analysis (Under Direction of Zdeněk Kopal): Tables of Supersonic Flow Around Cones. Tech. Rep. No. 1 (NOrd Contract No. 9169), M.I.T., 1947.

5. Staff of the Computing Section, Center of Analysis (Under Direction of Zdeněk Kopal): Tables of Supersonic Flow Around Yawing Cones. Tech. Rep. No. 3 (NOrd Contract No. 9169), M.I.T., 1947.

6. Staff of the Computing Section, Center of Analysis (Under Direction of Zdeněk Kopal): Tables of Supersonic Flow Around Cones of Large Yaw. Tech. Rep. No. 5 (NOrd Contracts Nos. 8555 and 9169), M.I.T., 1949.

7. Huston, Wilber B., and Skopinski, T. H.: Probability and Frequency Characteristics of Some Flight Buffet Loads. NACA TN 3733, 1956.

TABLE I.- LOCAL SKIN THICKNESS AND LOCATION OF THERMOCOUPLES AND PRESSURE ORIFICES

Thermocouple	$\frac{x}{l}$	Thickness, in.	Wire gage
1	0.05	0.0710	36
2	.07	.0315	
3	.08		
4	.13	.0310	
5	.17		
6	.21		
7	.24		
8	.28		
9	.32		
10	.36	.0315	
11	.40		
12	.44		
13	.48		
14	.52	.0320	
15	.55		
16	.59		
17	.63		
18	.67		
19	.71		
20	.75		
21	.79		
22	.83		
23	.86		
24	.24	.0310	30
25	.48	.0315	
26	.71	.0315	
27	.86	.0320	
28	.24	.0310	24
29	.48	.0315	
30	.71	.0310	
31	.86	.0320	
32	.24	.0315	36
33	.48	.0315	
34	.71	.0310	
35	.86	.0320	
36	.24	.0315	24
37	.48		
38	.71		
39	.86	.0320	
40	.24	.0315	30
41	.48		
42	.71		
43	.86	.0320	
44	.24	.0315	36
45	.48	.0315	
46	.71	.0315	
47	.86	.0320	

Static Pressure Orifices

	0.27 .90		

TABLE II.- TYPICAL LISTING OF HEAT-TRANSFER COEFFICIENTS USING THE INTEGRAL SOLUTION

$[M = 2.98;\ R = 1.79 \times 10^6;\ \alpha = 0^o;\ x/l = 0.52;\ \phi = 0^o$

$T_{w,t=0} = 567.1;\ T_e/T_t = 0.91964;\ t_o = 11.2\ ]$

t	$\sum_{t=t_o}^{t=t} T_w$	$wc(T_w - T_{w_o})$	T_w	h
13.2	1135.7	0.19098	568.5	0.00159
15.2	2273.6	.33952	569.5	.00137
17.2	3413.9	.48275	570.5	.00128
19.2	4556.3	.67904	571.8	.00134
21.2	5701.1	.82227	572.8	.00130
23.2	6848.2	1.01856	574.1	.00135
25.2	7997.3	1.16710	575.1	.00133
27.2	9148.8	1.31564	576.1	.00131
29.2	10302.4	1.45887	577.1	.00130
31.2	11458.1	1.66046	578.5	.00133
33.2	12615.9	1.80370	579.5	.00132
35.2	13775.9	1.95224	580.5	.00132

TABLE III. - RATE OF INCREASE OF HEAT TRANSFER WITH α.

$\frac{x}{l}$	$\frac{N_{St,\alpha=7.5^o}}{N_{St,\alpha=0^o}}$			$\frac{N_{St,\alpha=15^o}}{N_{St,\alpha=0^o}}$		
	ϕ			ϕ		
	0^o	120^o	180^o	0^o	120^o	180^o
M = 2.49; R = 1.71 x 10^6						
0.24	2.2	1.2	2.0	2.4	1.3	1.6
.48	2.2	1.0	3.0	2.7	1.2	2.1
.71	2.5	1.7	3.2	3.1	2.0	2.2
.86	2.1		3.6	2.6		2.3
M = 2.49; R = 3.63 x 10^6						
0.24	1.8	1.3	1.9	3.2	1.7	2.2
.48	1.9	3.0	2.7	3.4	2.5	2.7
.71	.3	.8	1.7	.6	.7	1.8
.86	.3		.7	.6		1.1
M = 2.98; R = 1.83 x 10^6						
0.24	2.3	1.3	1.9	3.0	1.5	1.9
.48	2.6	1.2	3.2	3.7	1.4	2.7
.71	3.3	1.6	3.8	4.7	2.1	3.0
.86	3.4		5.2	4.9		3.9
M = 2.98; R = 4.04 x 10^6						
0.24	2.0	1.4	2.4	3.0		2.1
.48	1.9	2.1	4.6	3.0	2.7	3.8
.71	.4	.7	.8	.7	.5	.6
.86	.2		.9	.6		.6
M = 3.51; R = 1.89 x 10^6						
0.24	2.2		1.2	3.0		1.4
.48	2.3	1.0	2.3	3.2	1.9	1.9
.71	1.6	1.1	2.9	4.7	1.9	2.1
.86	.3		4.2	.8		3.2
M = 3.51; R = 3.74 x 10^6						
0.24	2.1		1.7	3.2		1.6
.48	1.0	3.4	3.0	1.4	2.2	2.4
.71	.5	.8	.9	.8	.5	.7
.86	.5		.8	.7		.5
M = 3.96; R = 1.99 x 10^6						
0.24	2.4		1.3	3.3		1.4
.48	2.5	1.0	2.5	3.6	0.9	2.1
.71	4.0	1.0	3.7	6.0	.8	2.8
.86	1.0		2.0	1.5		1.6
M = 3.96; R = 3.63 x 10^6						
0.24	2.4		1.7	3.8		1.6
.48	3.4	3.4	6.8	5.5	2.0	2.9
.71	.6	.7	.7	.9	.3	.5
.86	.6		.8	.9		.6
M = 4.65; R = 2.26 x 10^6						
0.24				3.2		1.4
.48					0.6	.9
.71				2.6	.4	.7
.86				2.7		.5

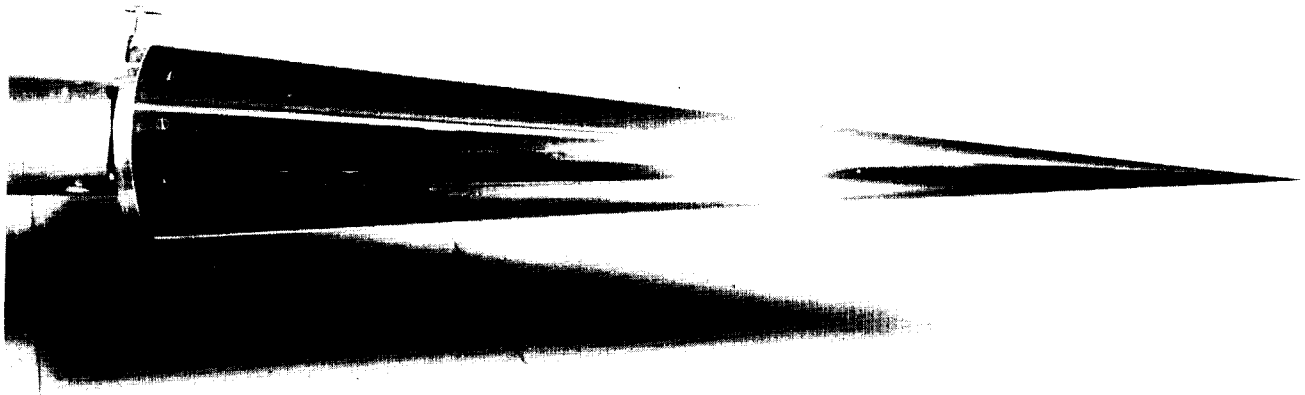

L-57-3150

Figure 1.- Thin-walled 10° cone installed in the Langley Unitary Plan wind tunnel.

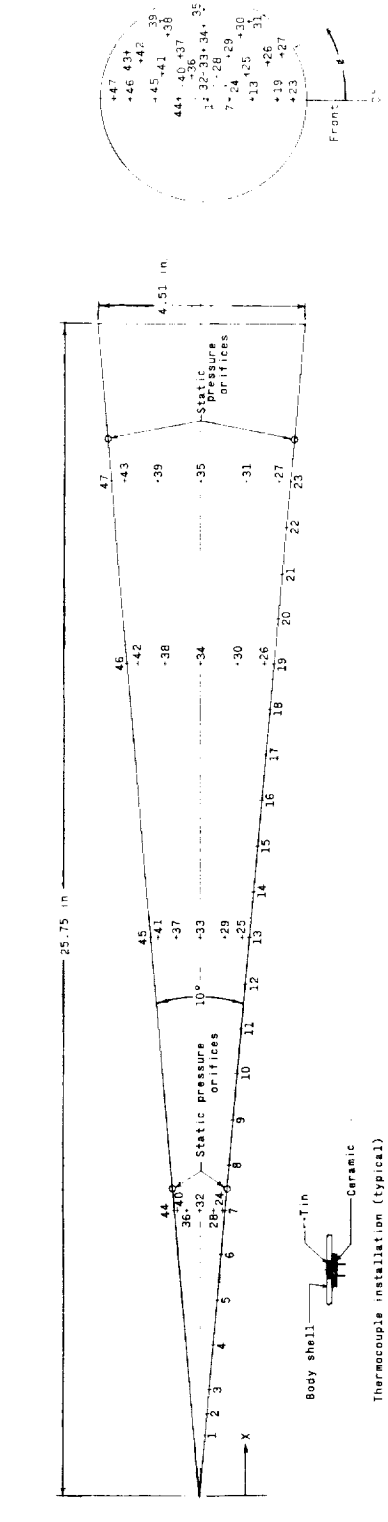

Figure 2.- Thermocouple and static orifice locations on the 10° cone.

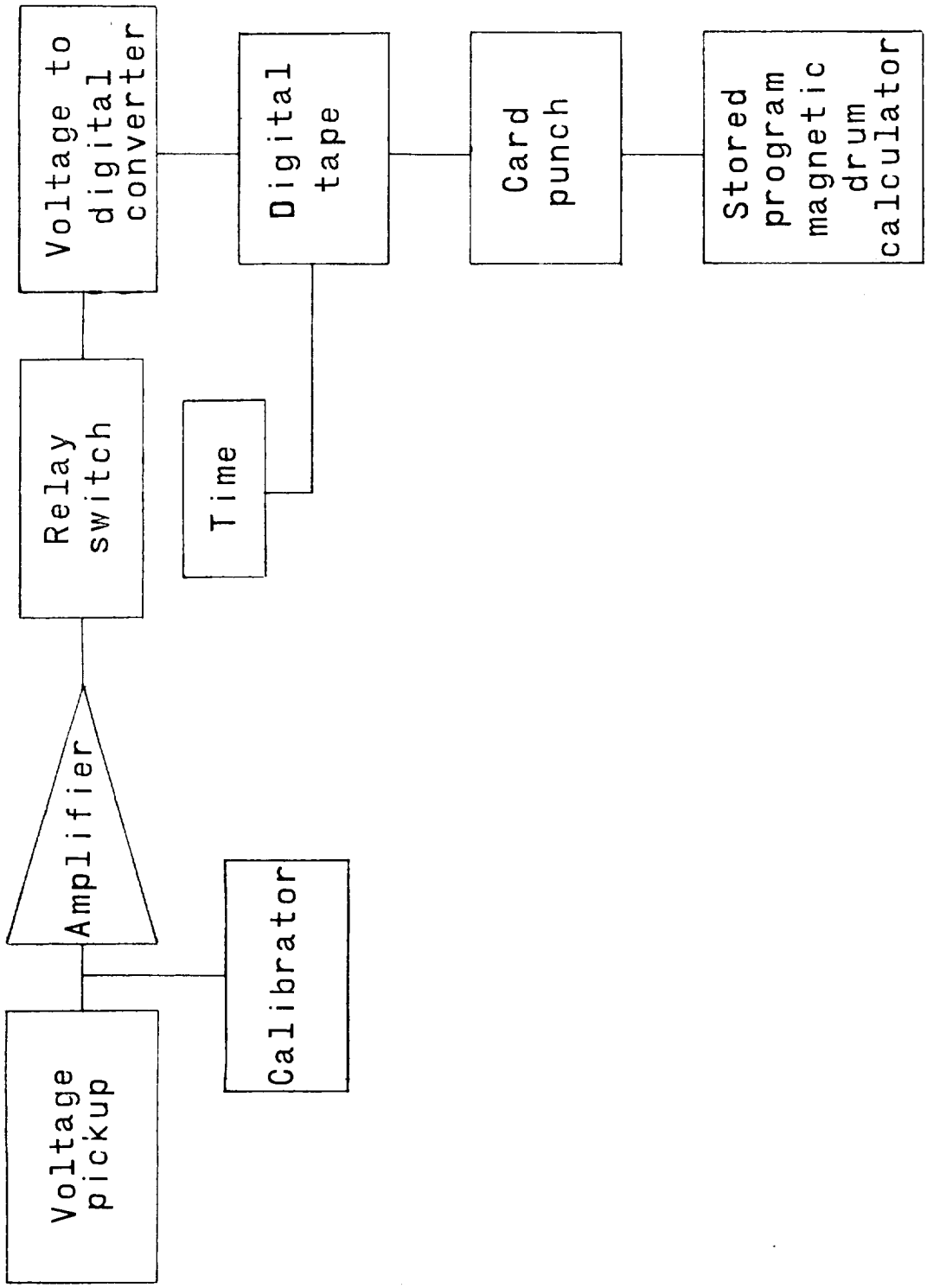

Figure 3.- Block diagram of multichannel sequential analog to digital conversion system.

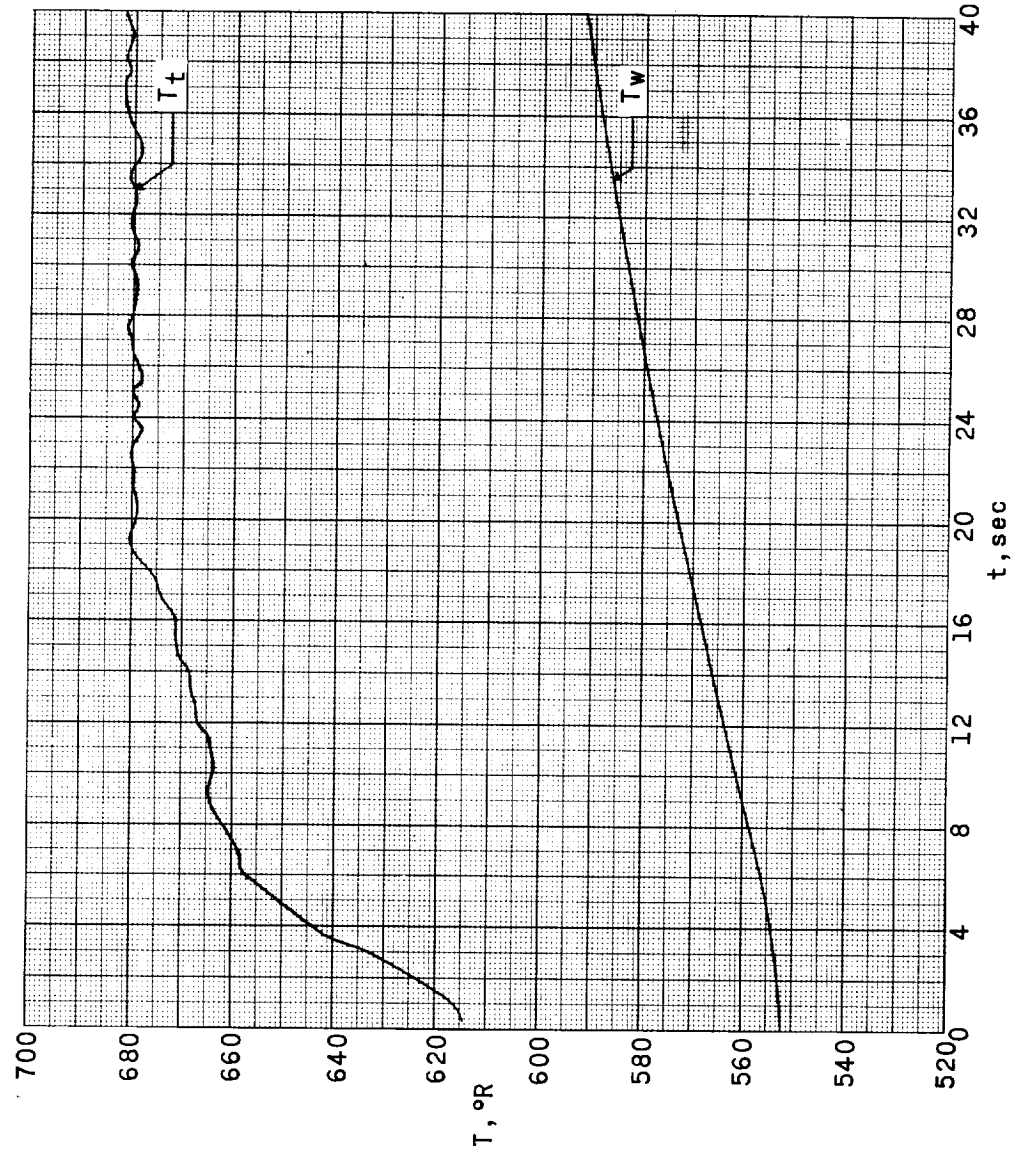

(a) M = 2.49; R = 3.42×10^6.

Figure 4.- Typical temperature-time history measured on the 10^o cone. $x/l = 0.24$.

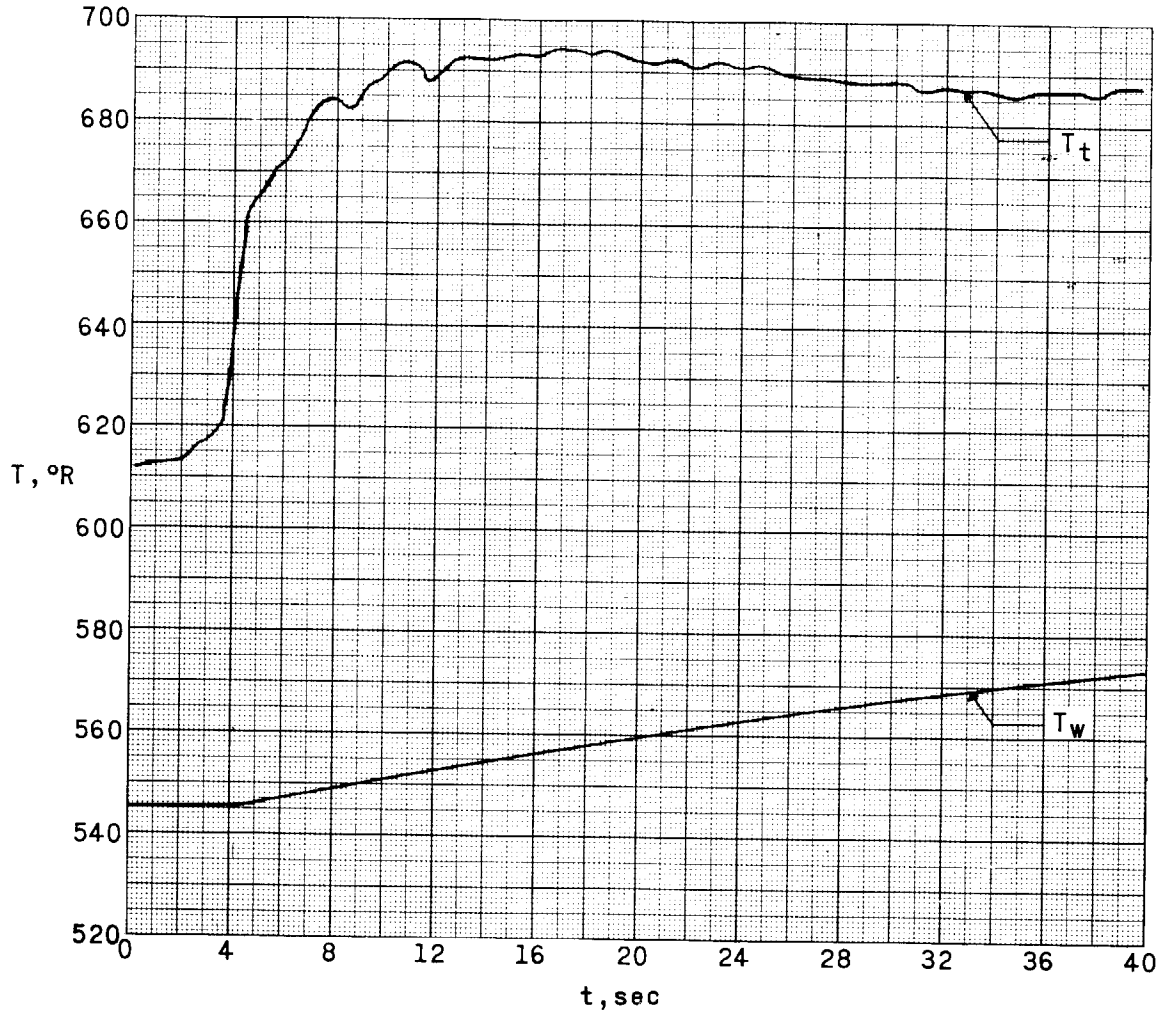

(b) $M = 3.96$; $R = 3.58 \times 10^6$.

Figure 4.- Concluded.

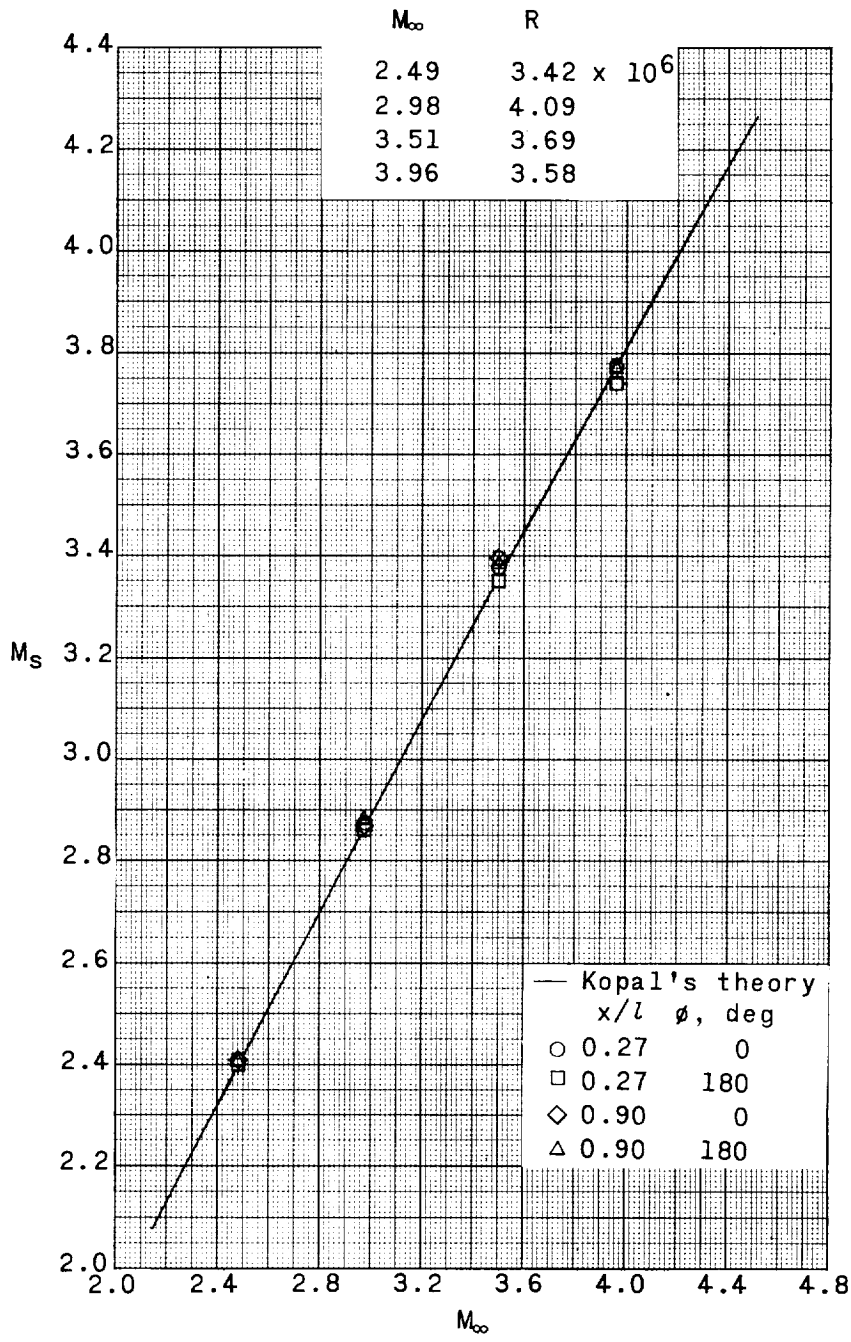

(a) $\alpha = 0^\circ$.

Figure 5.- Surface Mach numbers determined from static pressures measured on the 10° cone.

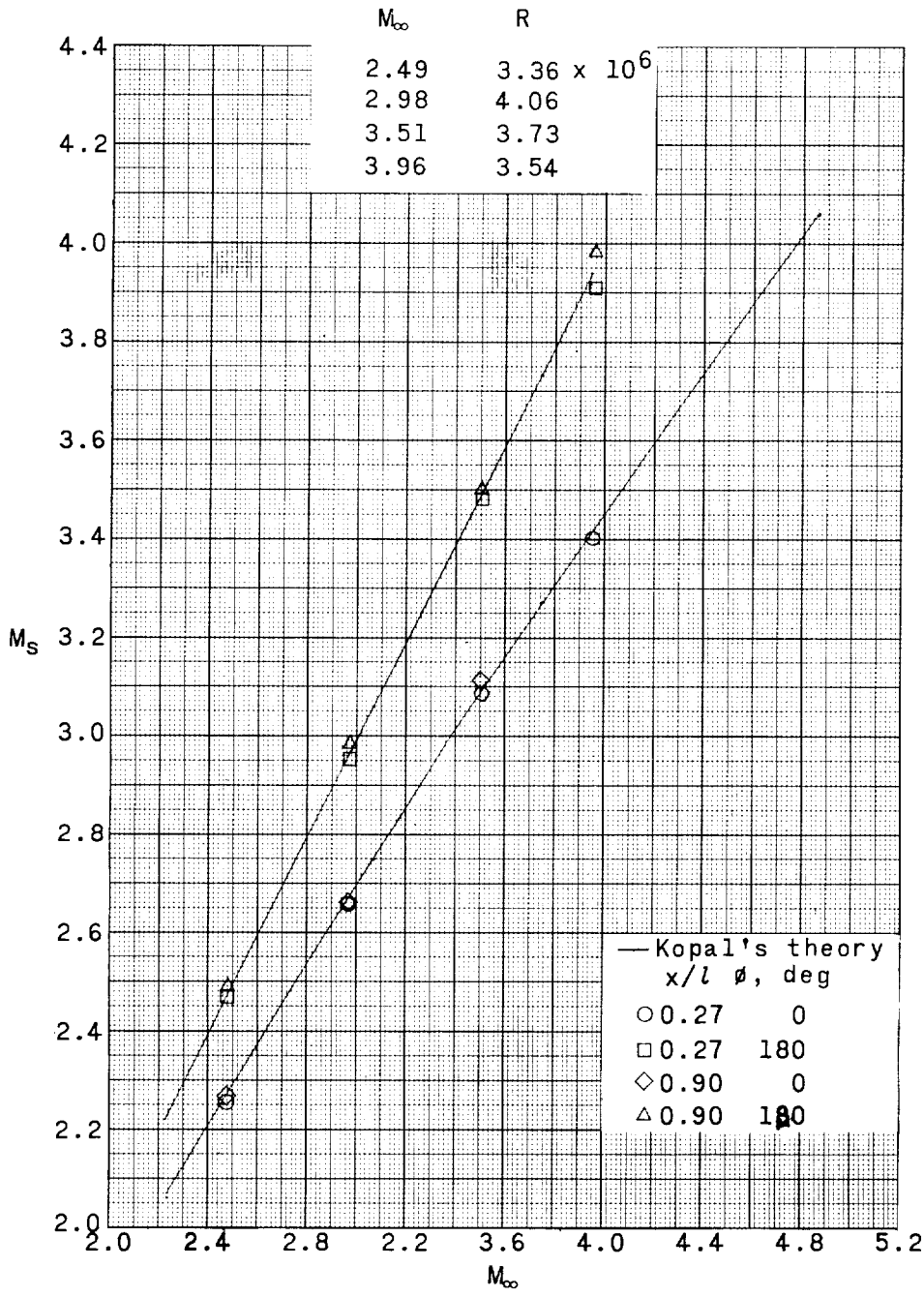

(b) $\alpha = 7.5^\circ$.

Figure 5.- Continued.

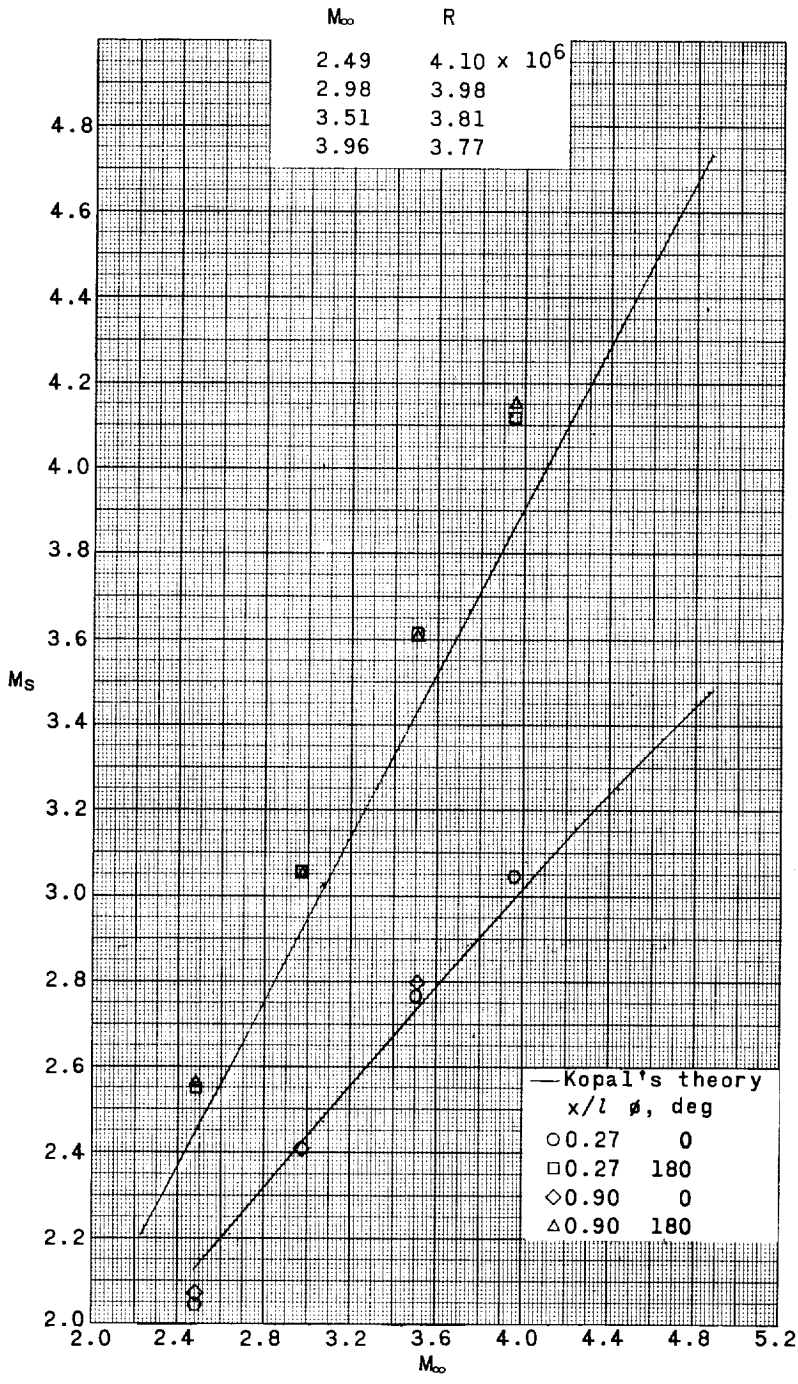

(c) $\alpha = 15^{\circ}$.

Figure 5.- Concluded.

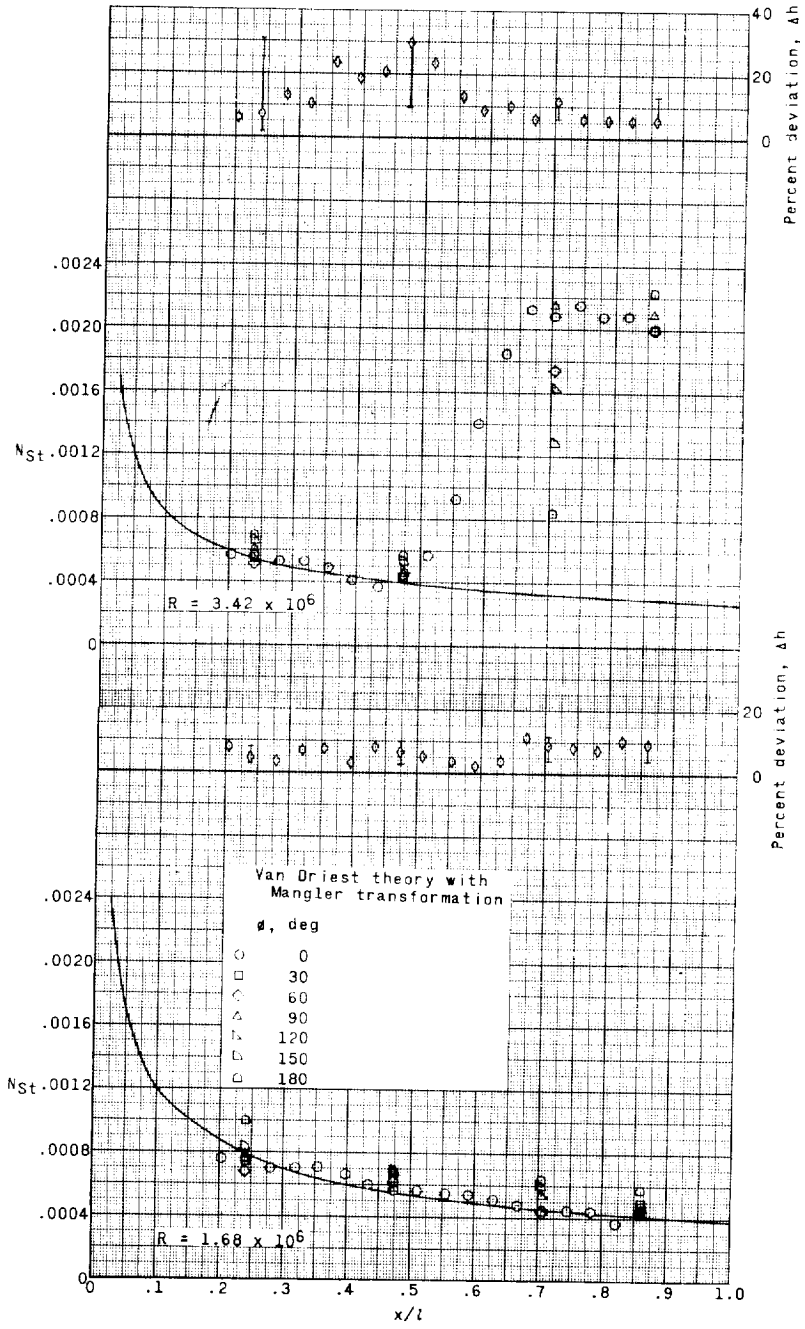

(a) M = 2.49.

Figure 6.- Distribution of heat-transfer coefficients on the 10° cone at an angle of attack of 0°.

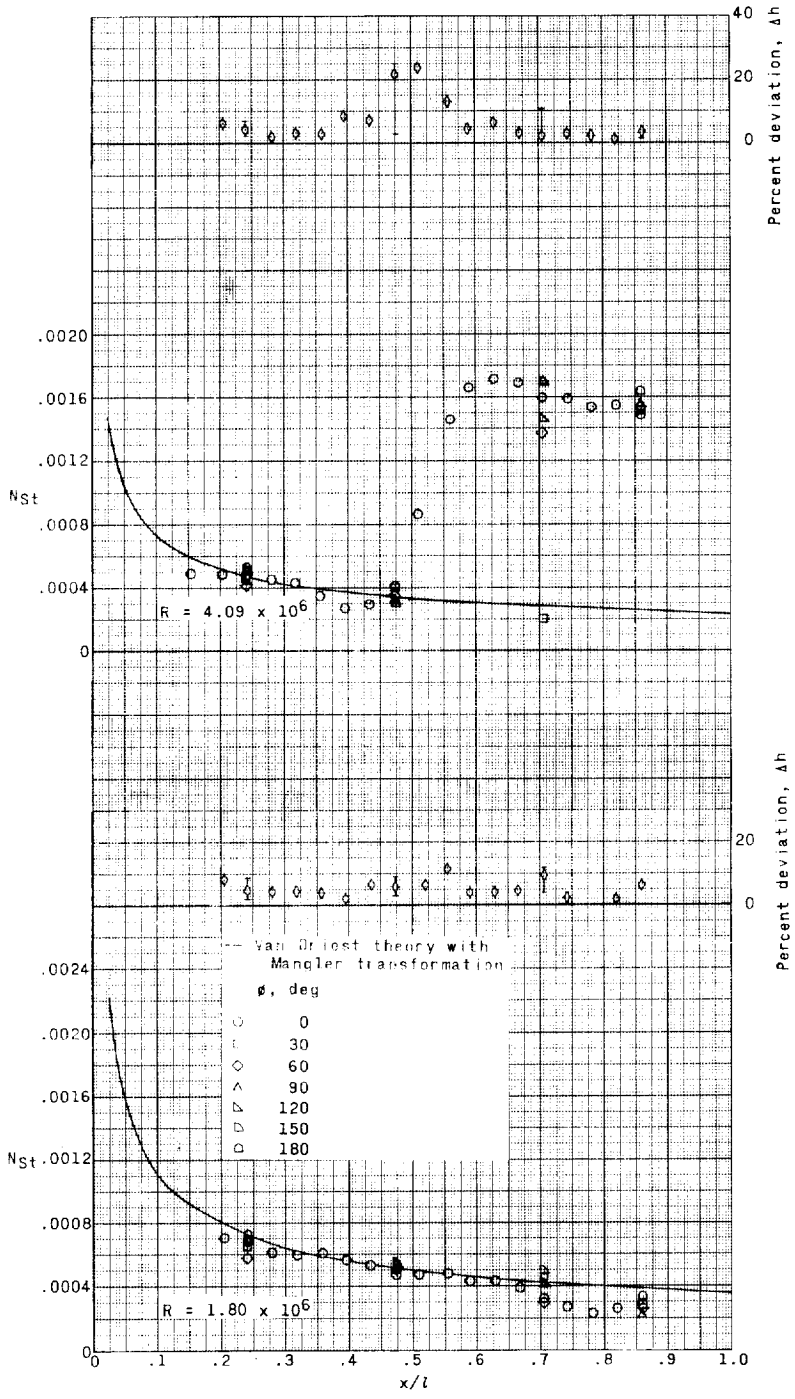

(b) M = 2.98.

Figure 6.- Continued.

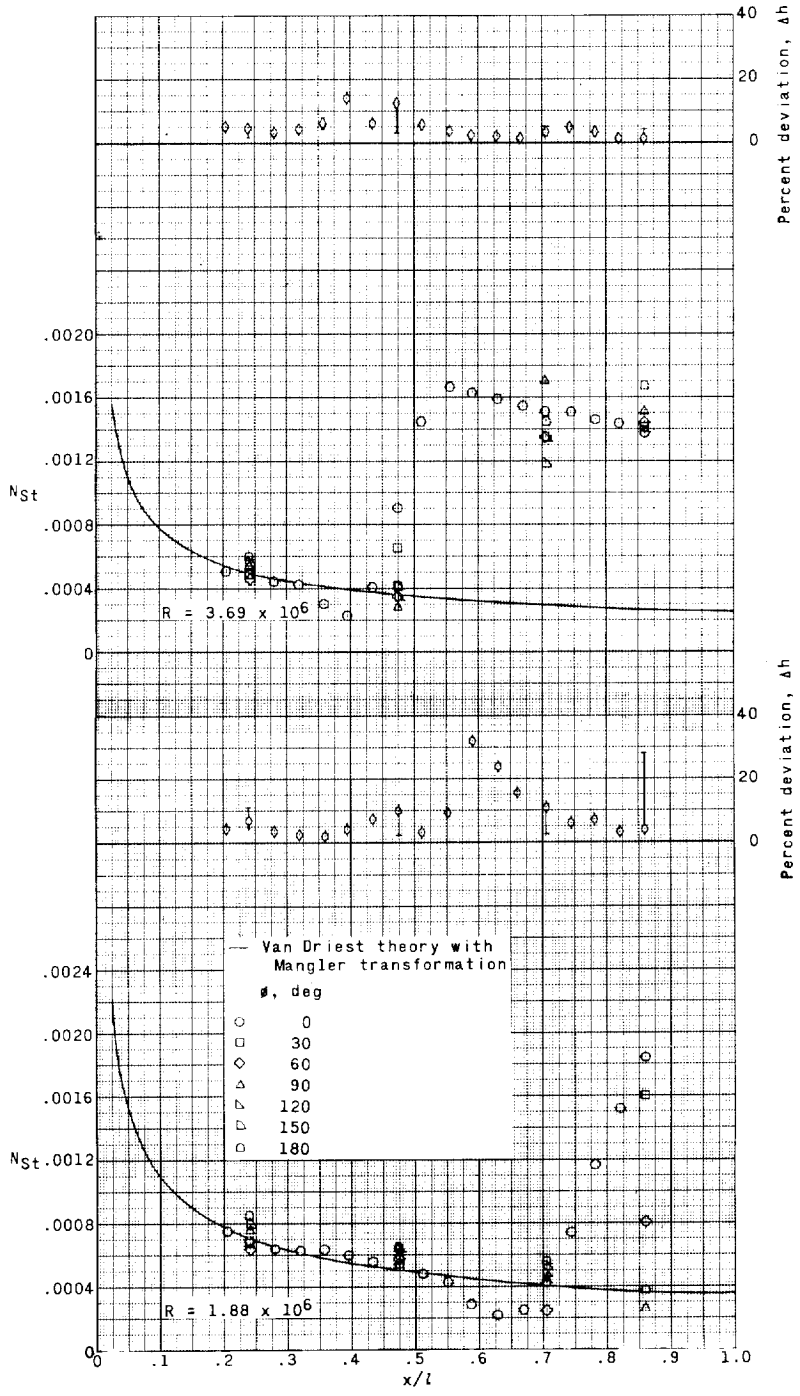

(c) M = 3.51.

Figure 6.- Continued.

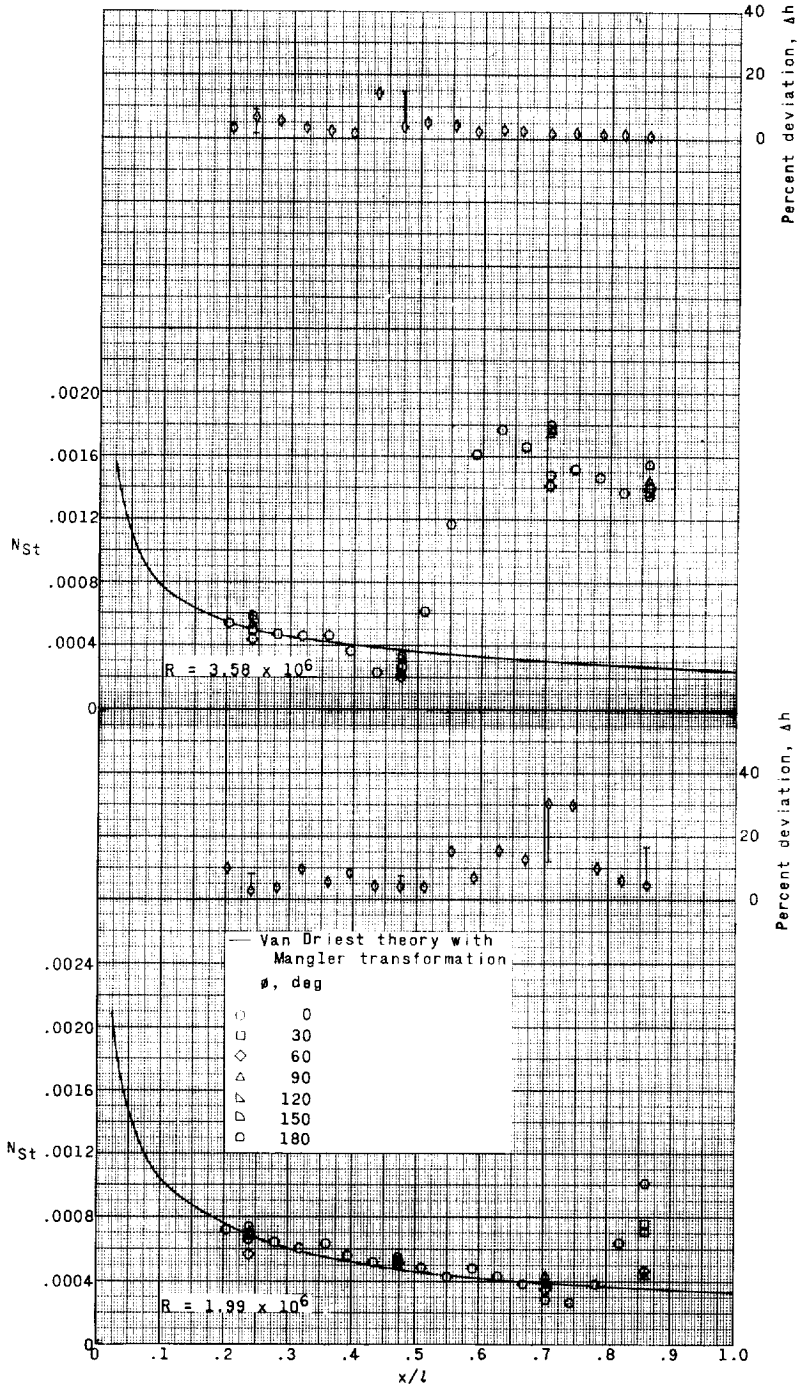

(d) M = 3.96.

Figure 6.- Continued.

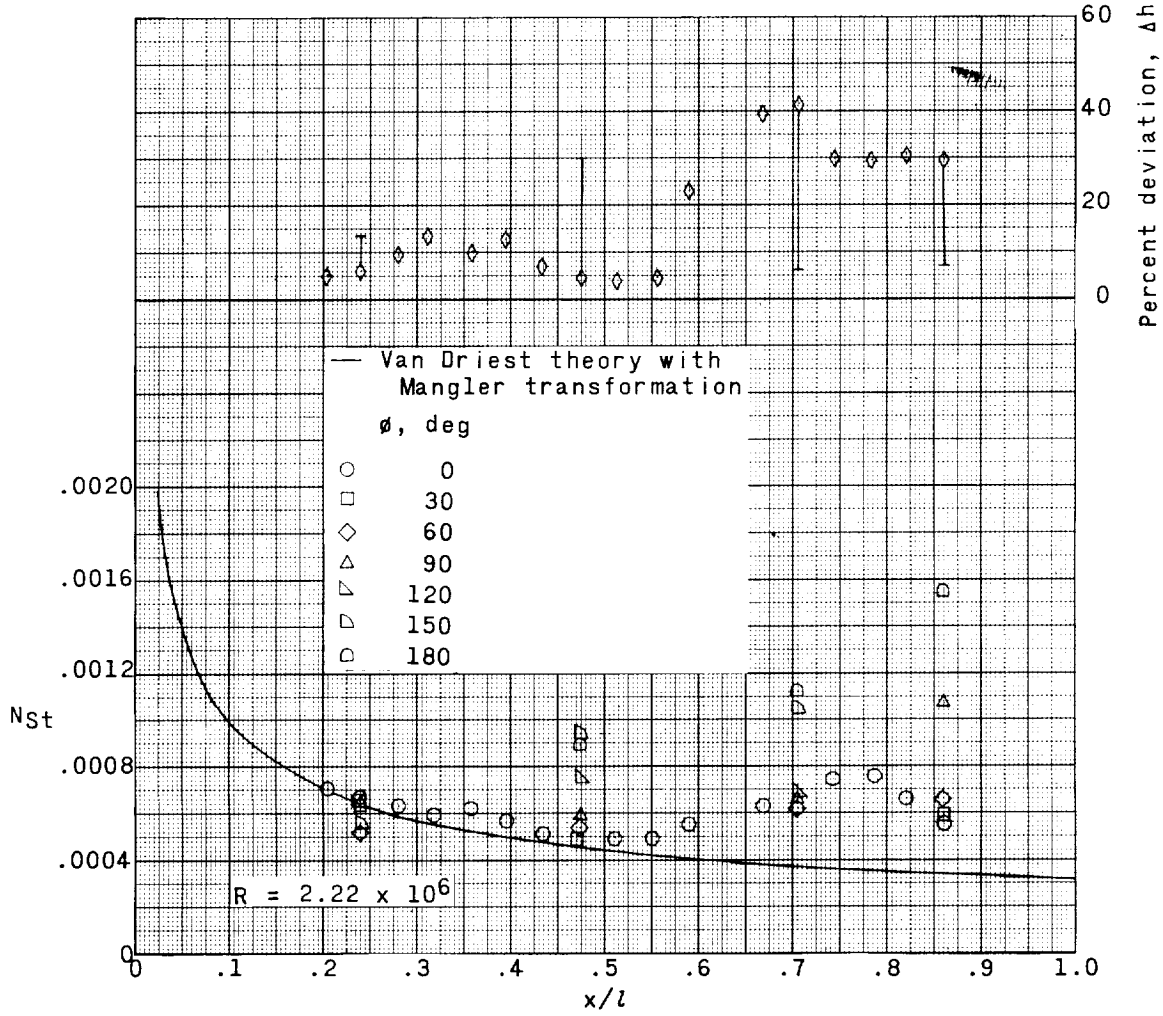

(e) M = 4.65.

Figure 6.- Concluded.

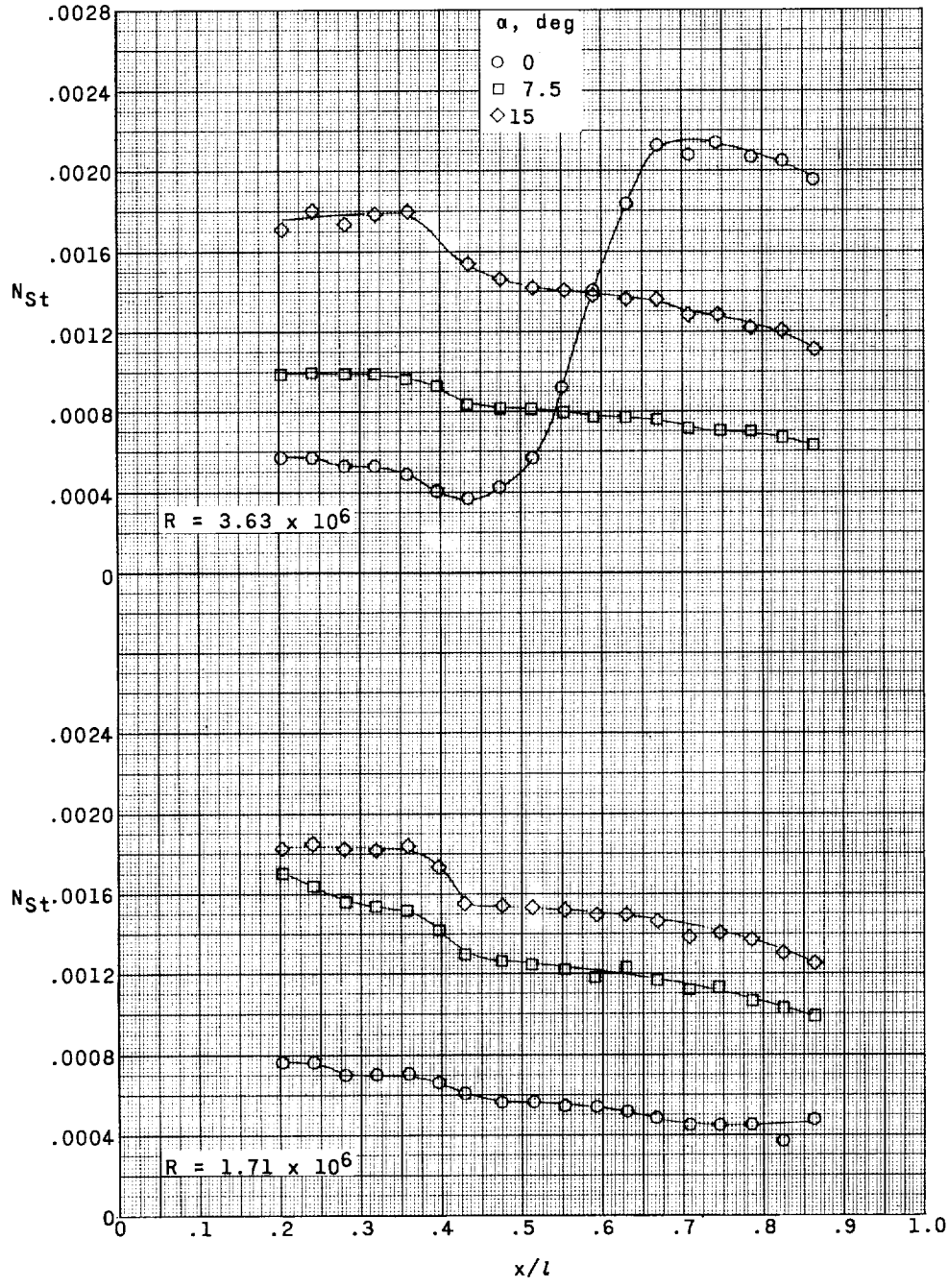

(a) M = 2.49.

Figure 7.- Effect of angle of attack on the distribution of heat-transfer coefficients on the 10° cone. $\phi = 0°$.

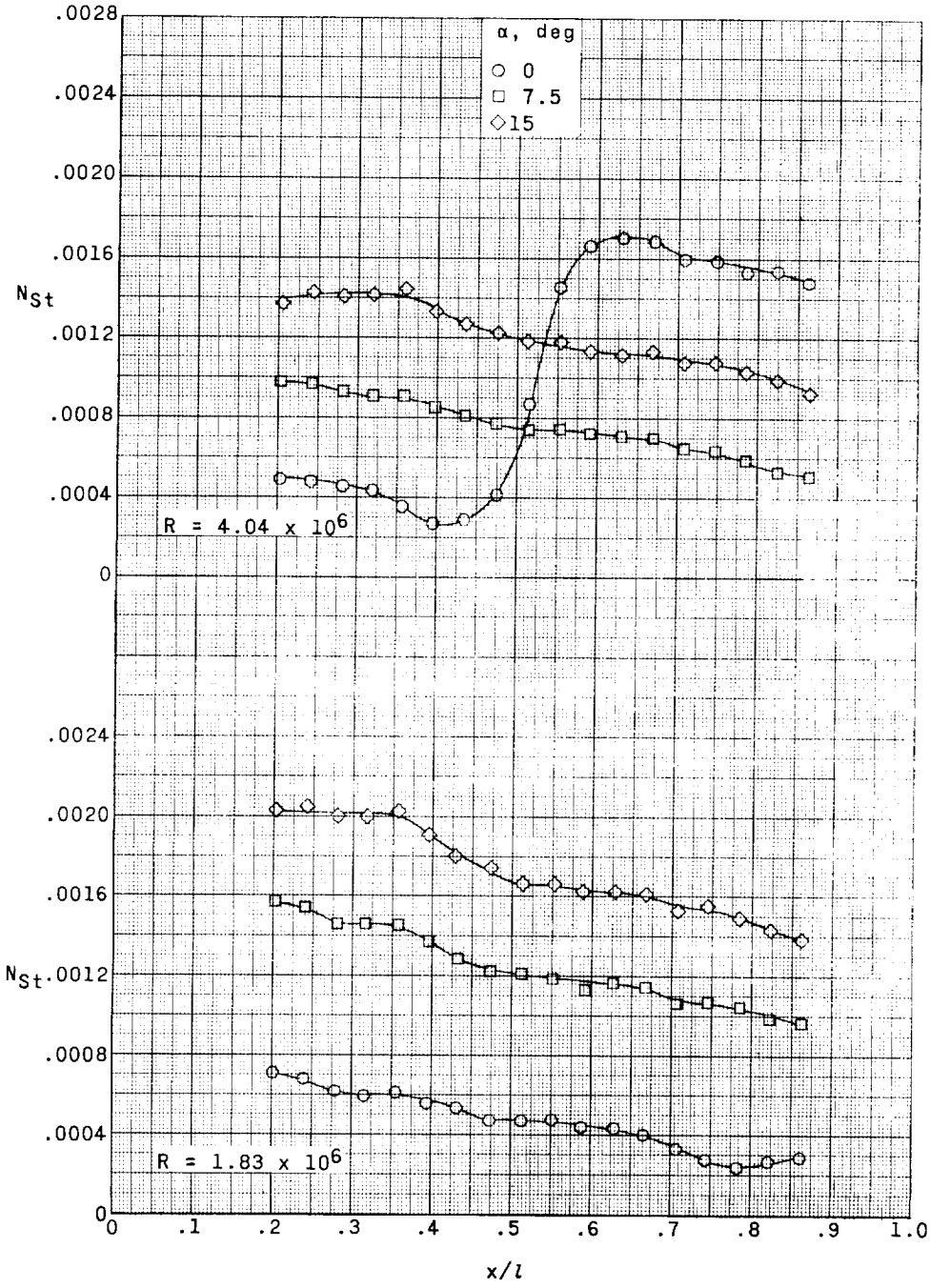

(b) M = 2.98.

Figure 7.- Continued.

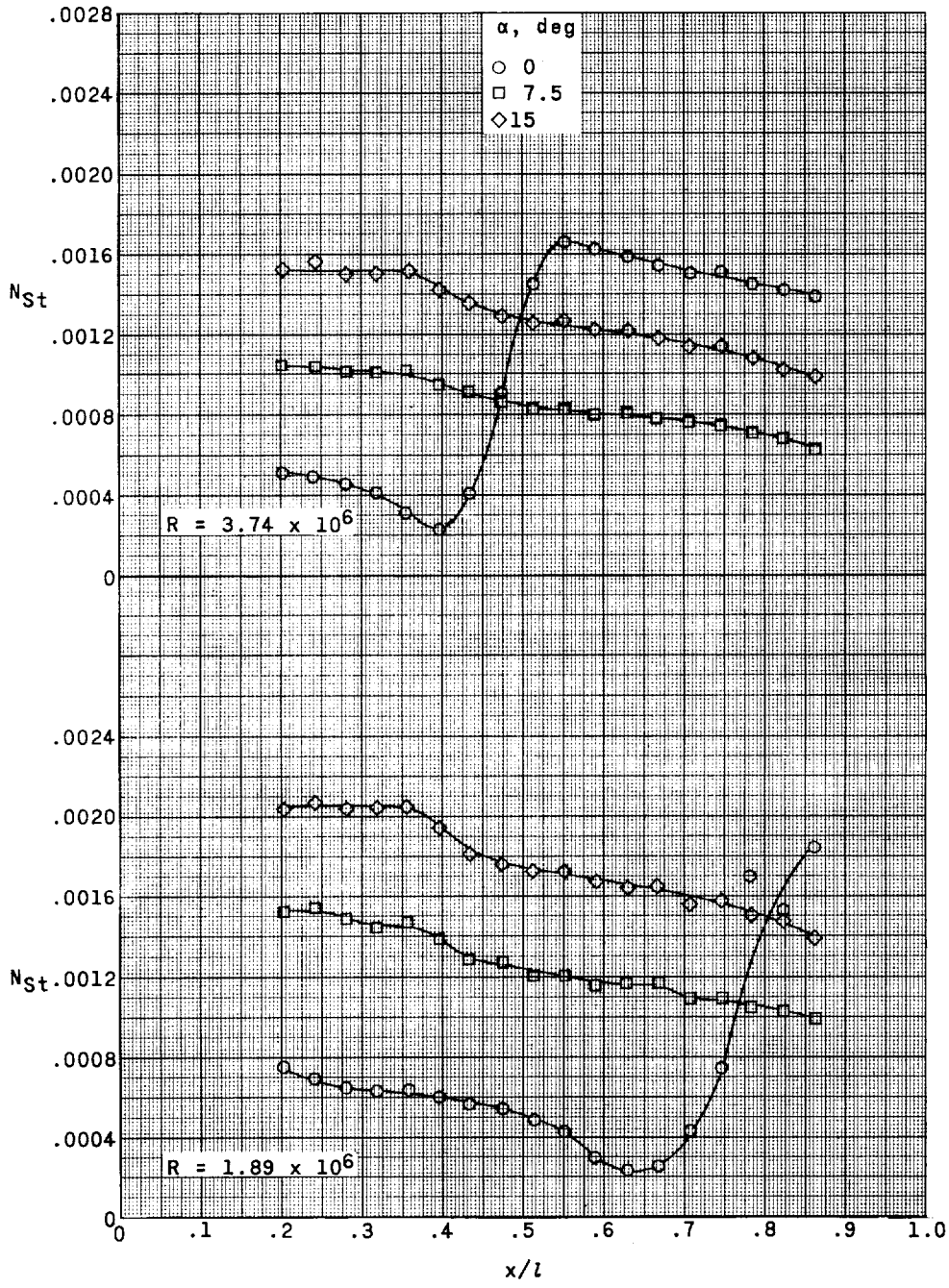

(c) M = 3.51.

Figure 7.- Continued.

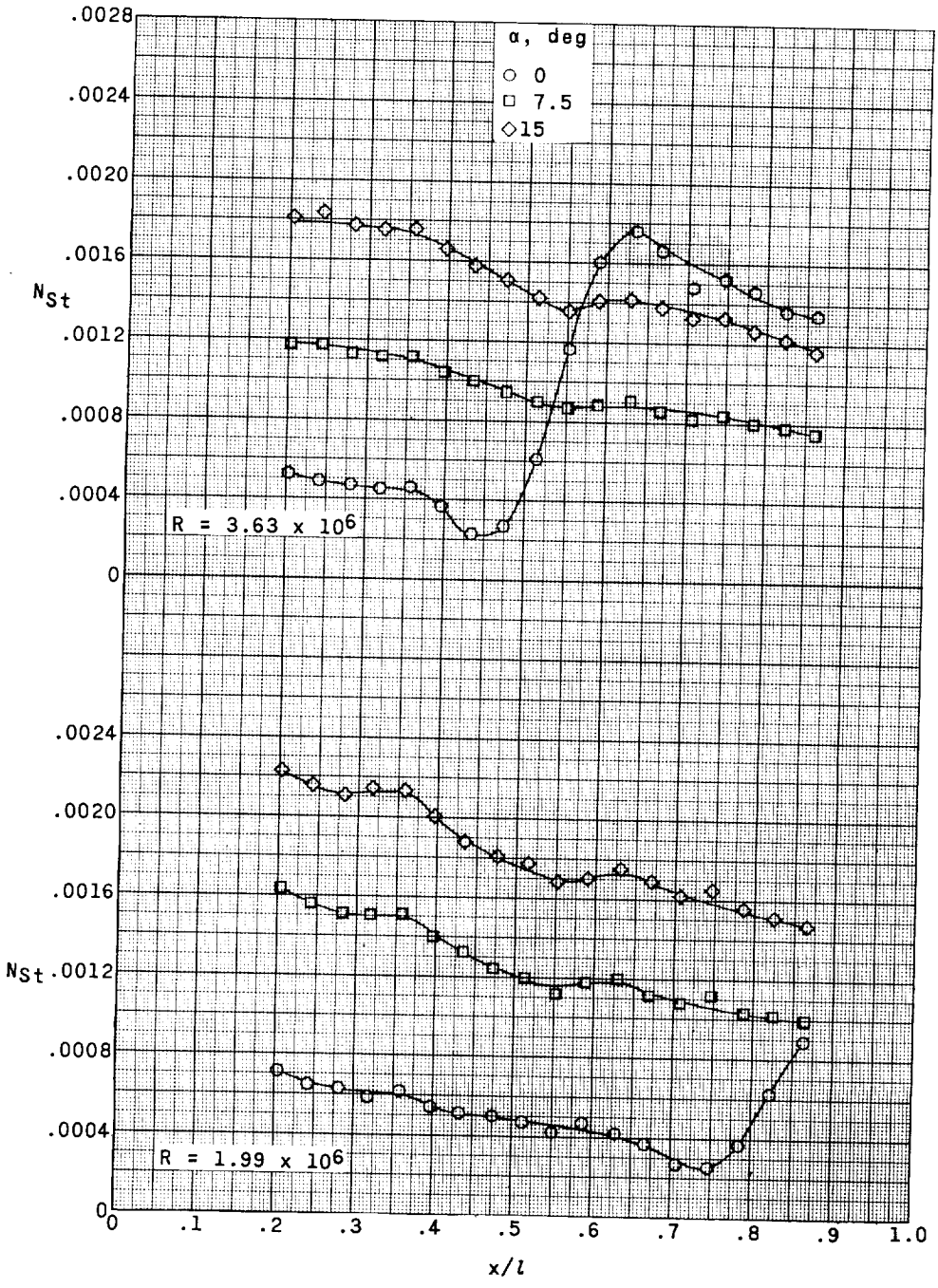

(d) M = 3.96.

Figure 7.- Continued.

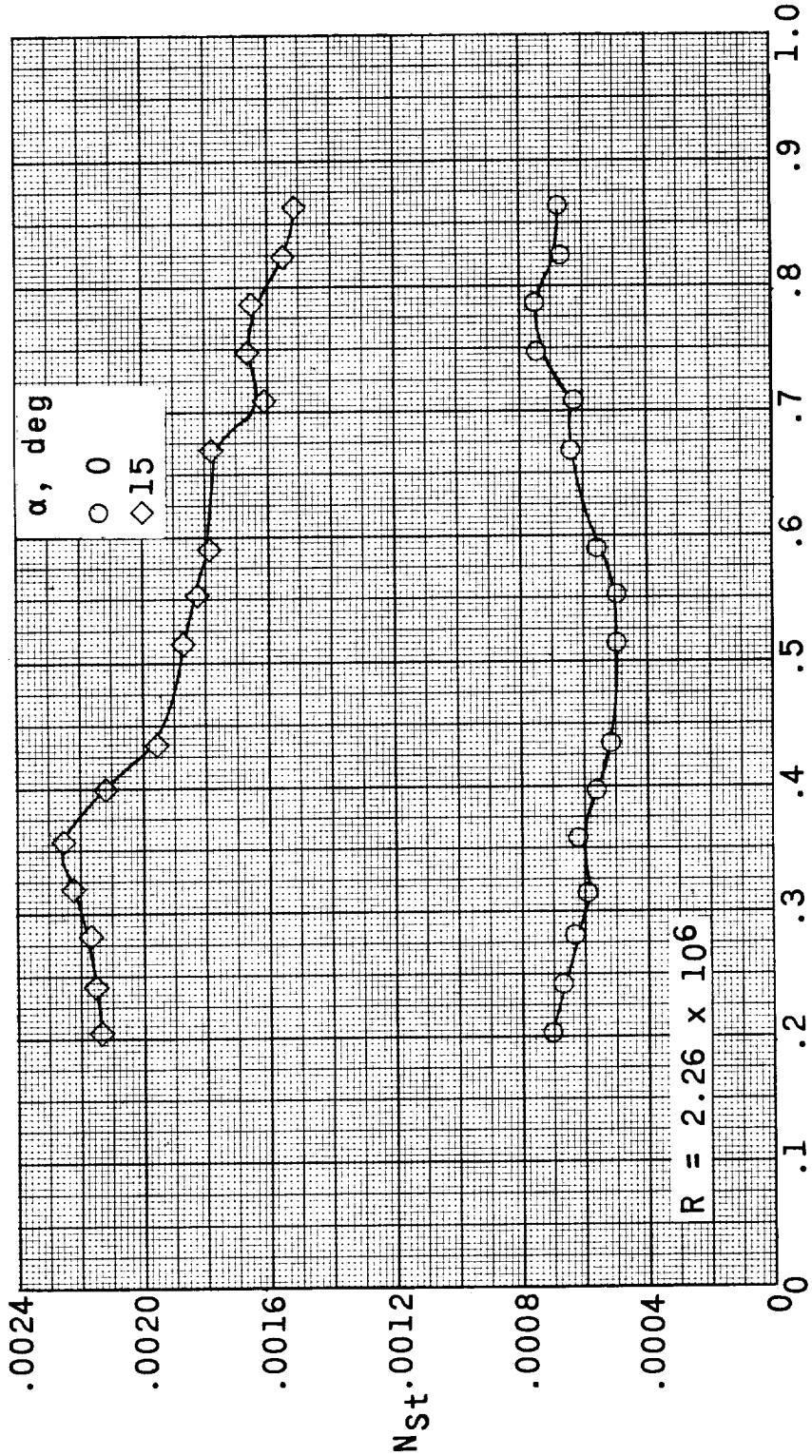

(e) M = 4.65.

Figure 7.- Concluded.

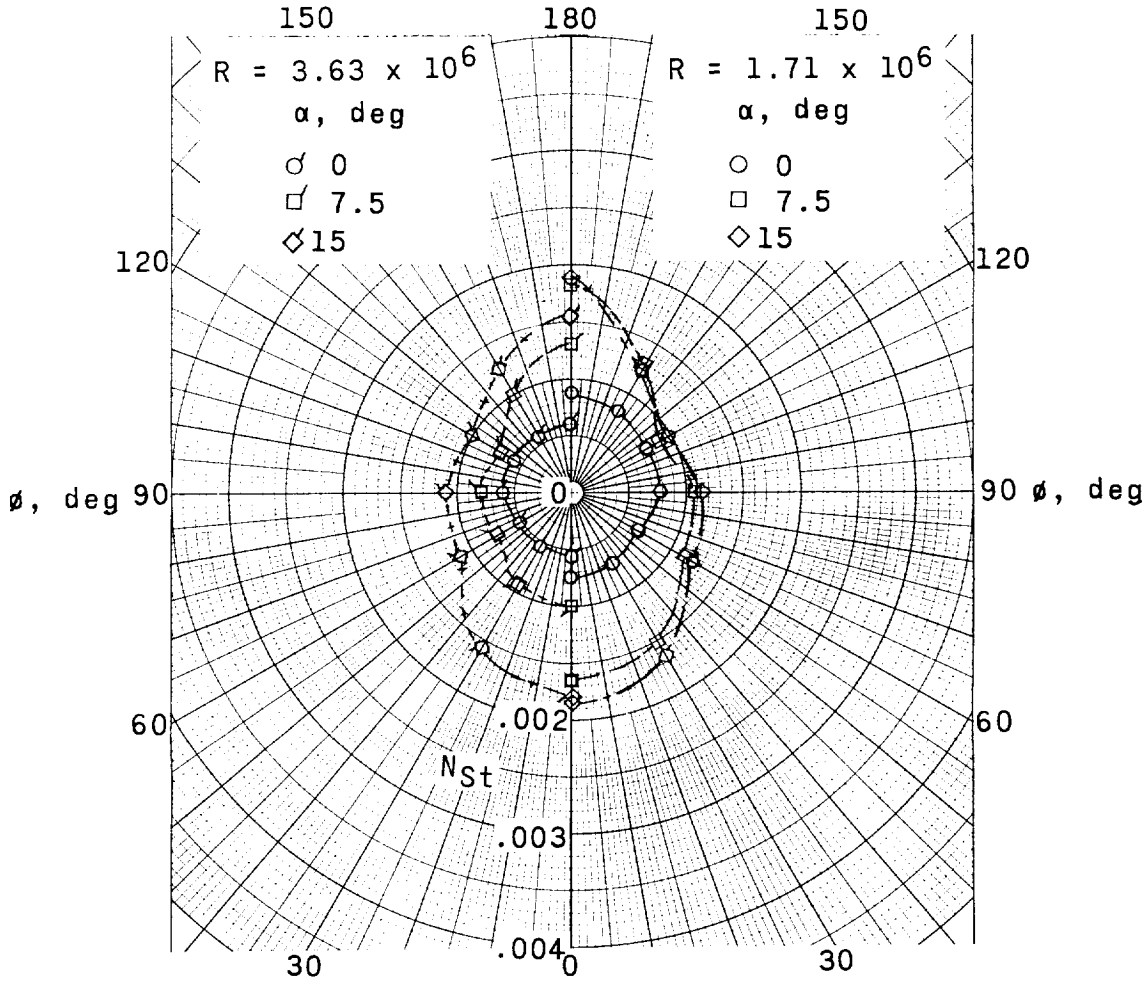

(a) $x/l = 0.24$.

Figure 8.- Effect of angle of attack on heat-transfer coefficients at various meridian angles of the 10° cone. M = 2.49. The high Reynolds number range was 3.36×10^6 to 4.10×10^6; the low Reynolds number range, 1.68×10^6 to 2.30×10^6.

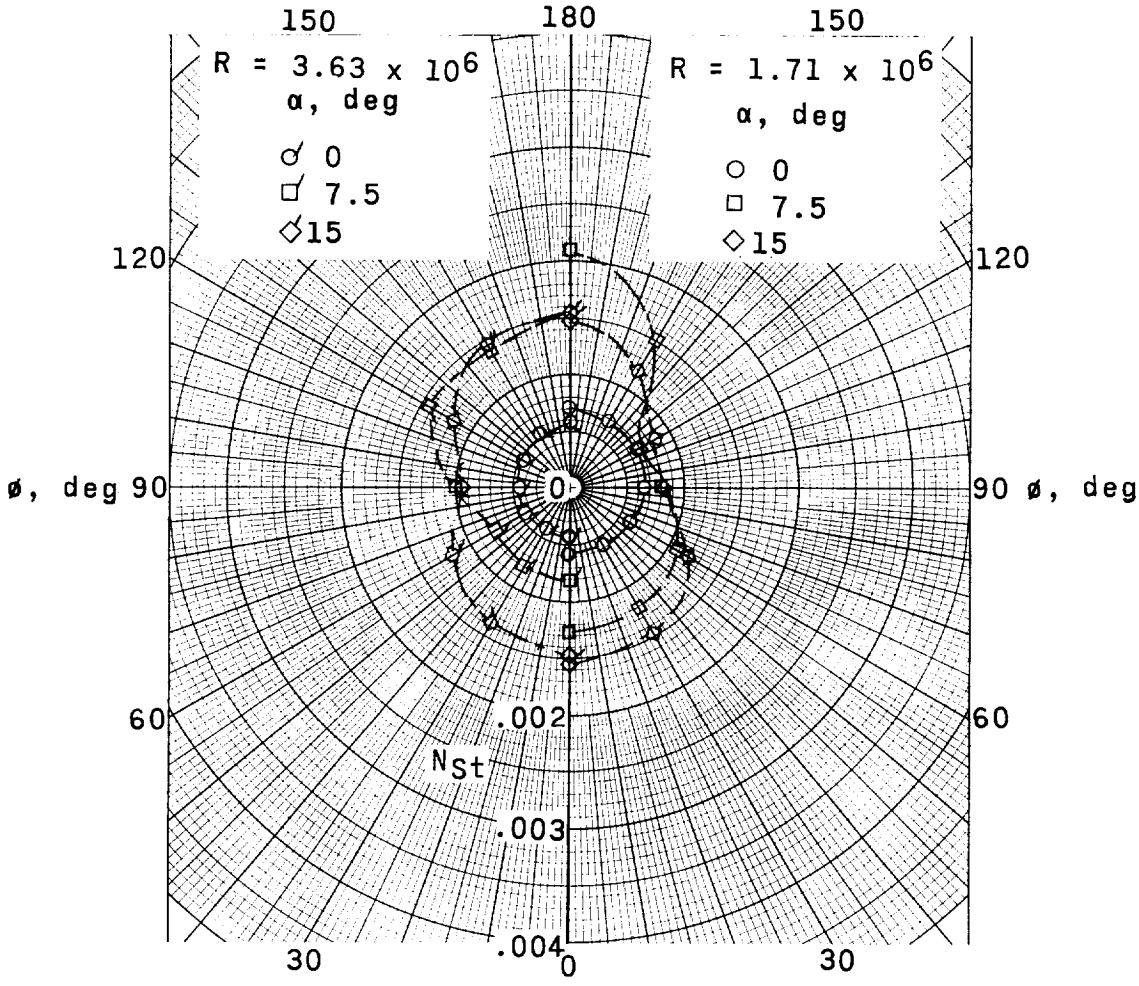

(b) $x/l = 0.48$.

Figure 8.- Continued.

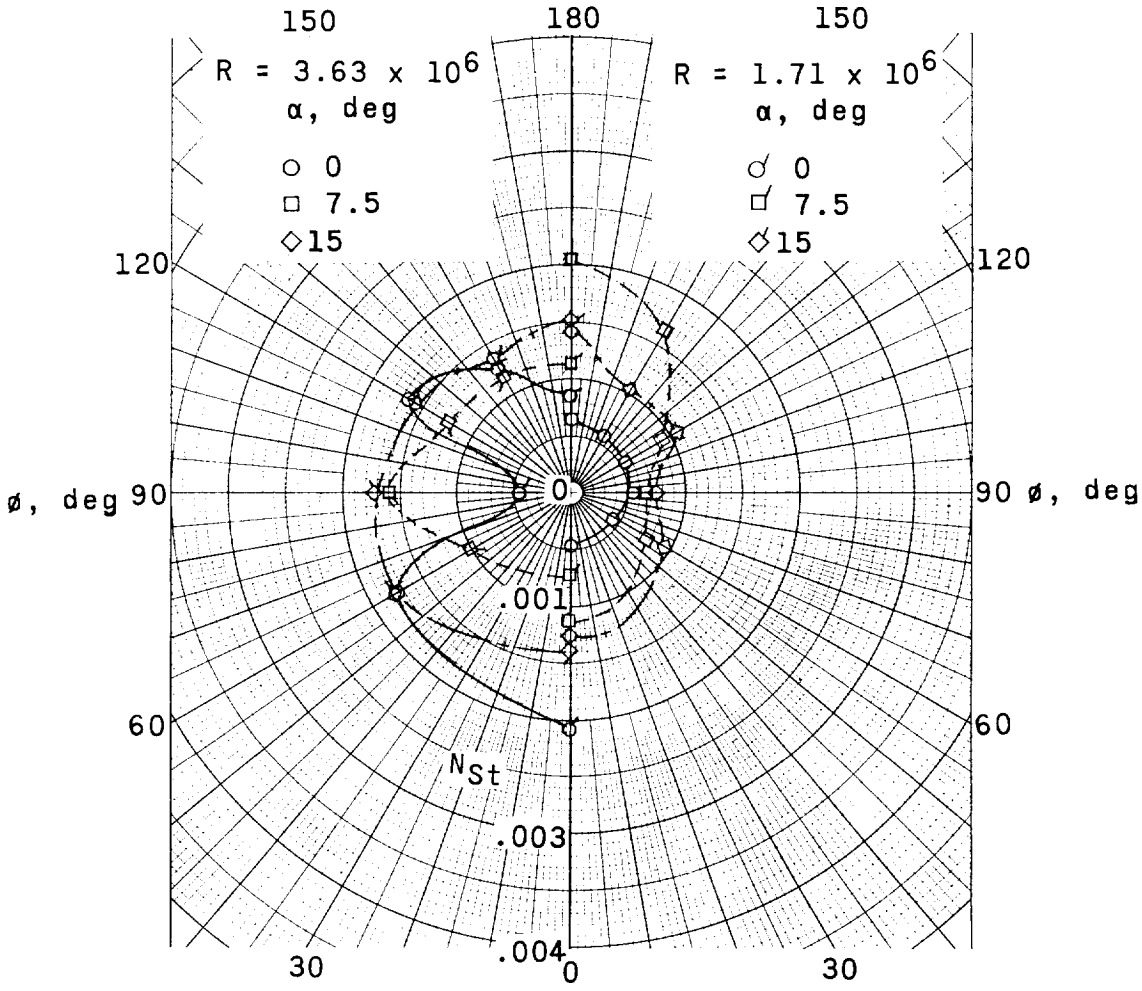

(c) $x/l = 0.71$.

Figure 8.- Continued.

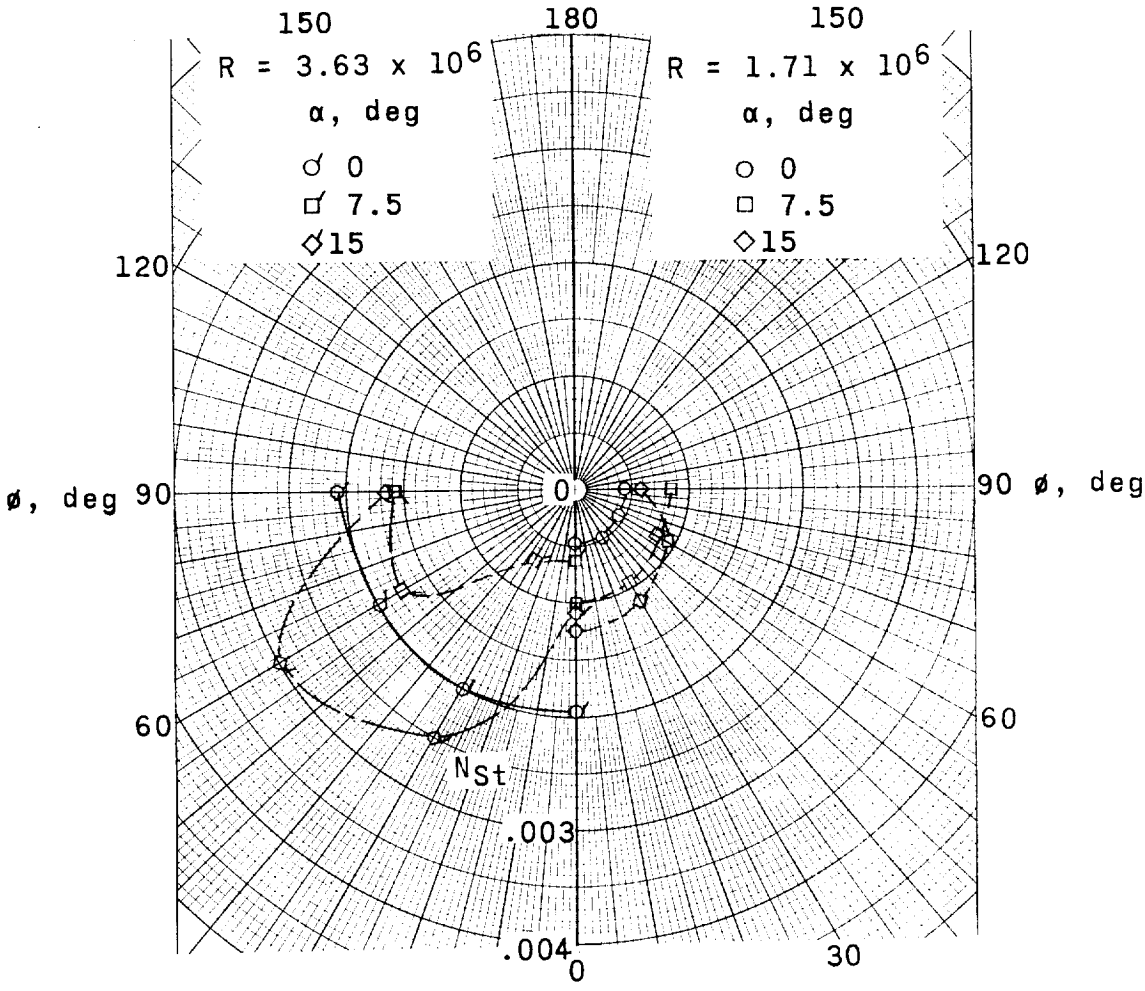

(d) $x/l = 0.86$.

Figure 8.- Concluded.

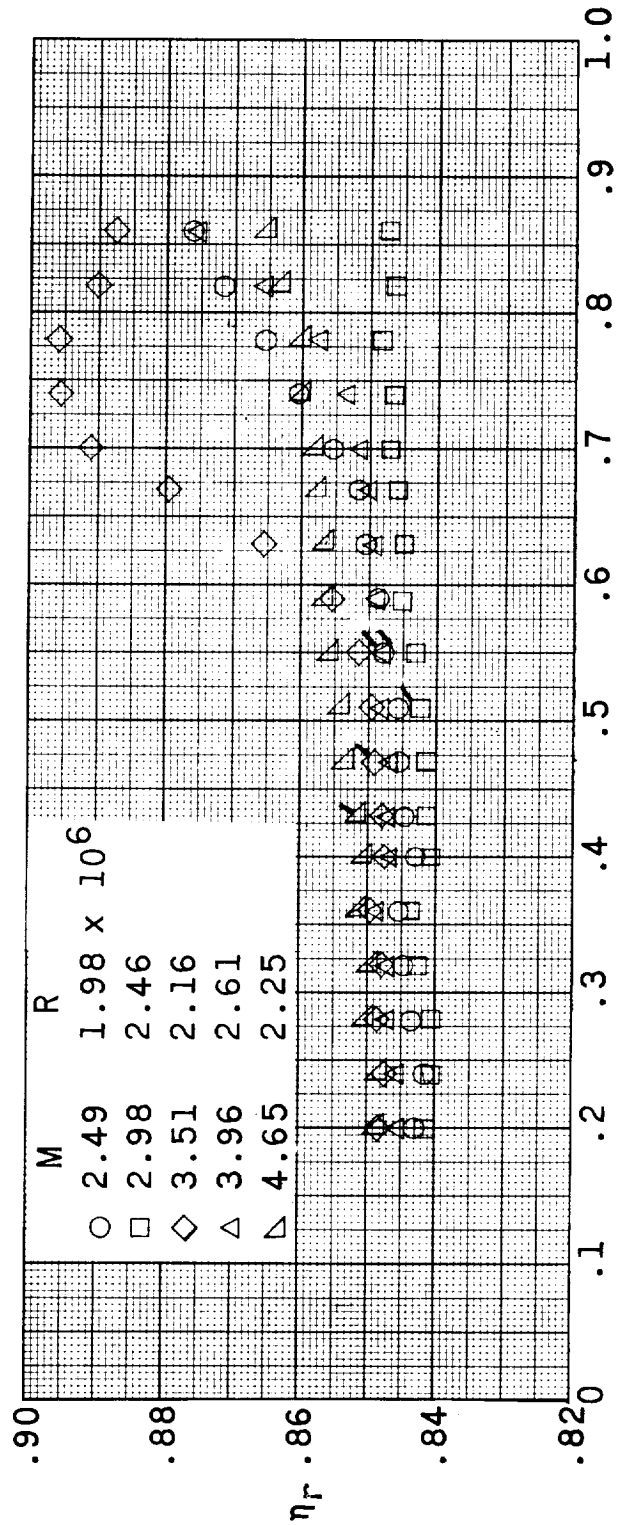

Figure 9.- Measured recovery factors on the 10° cone. $\phi = 0^{\circ}$. Flagged symbols denote transition length.

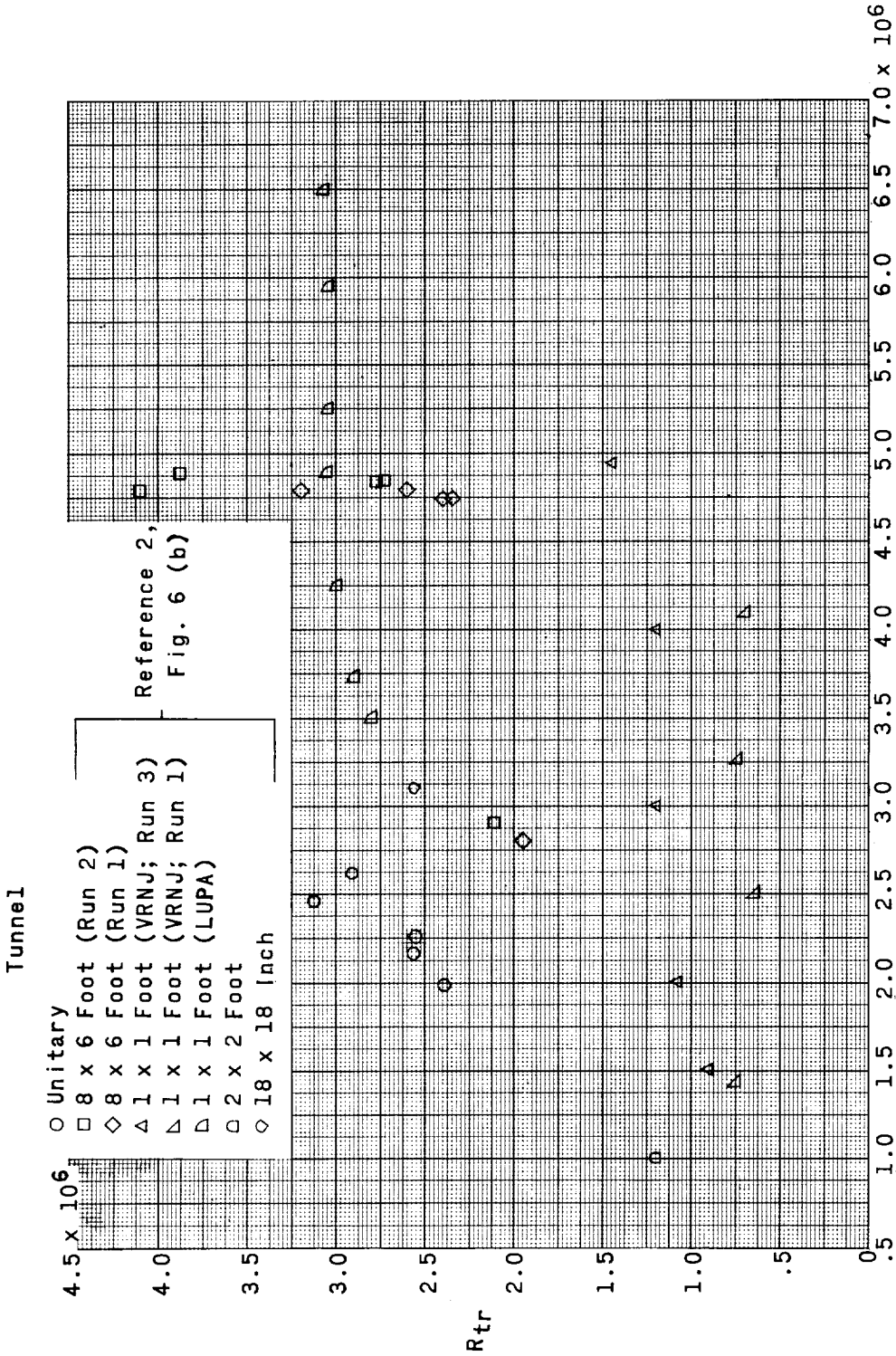

Figure 10.- Variation of R_{tr} with R_∞ for 10° cones tested in various tunnels.

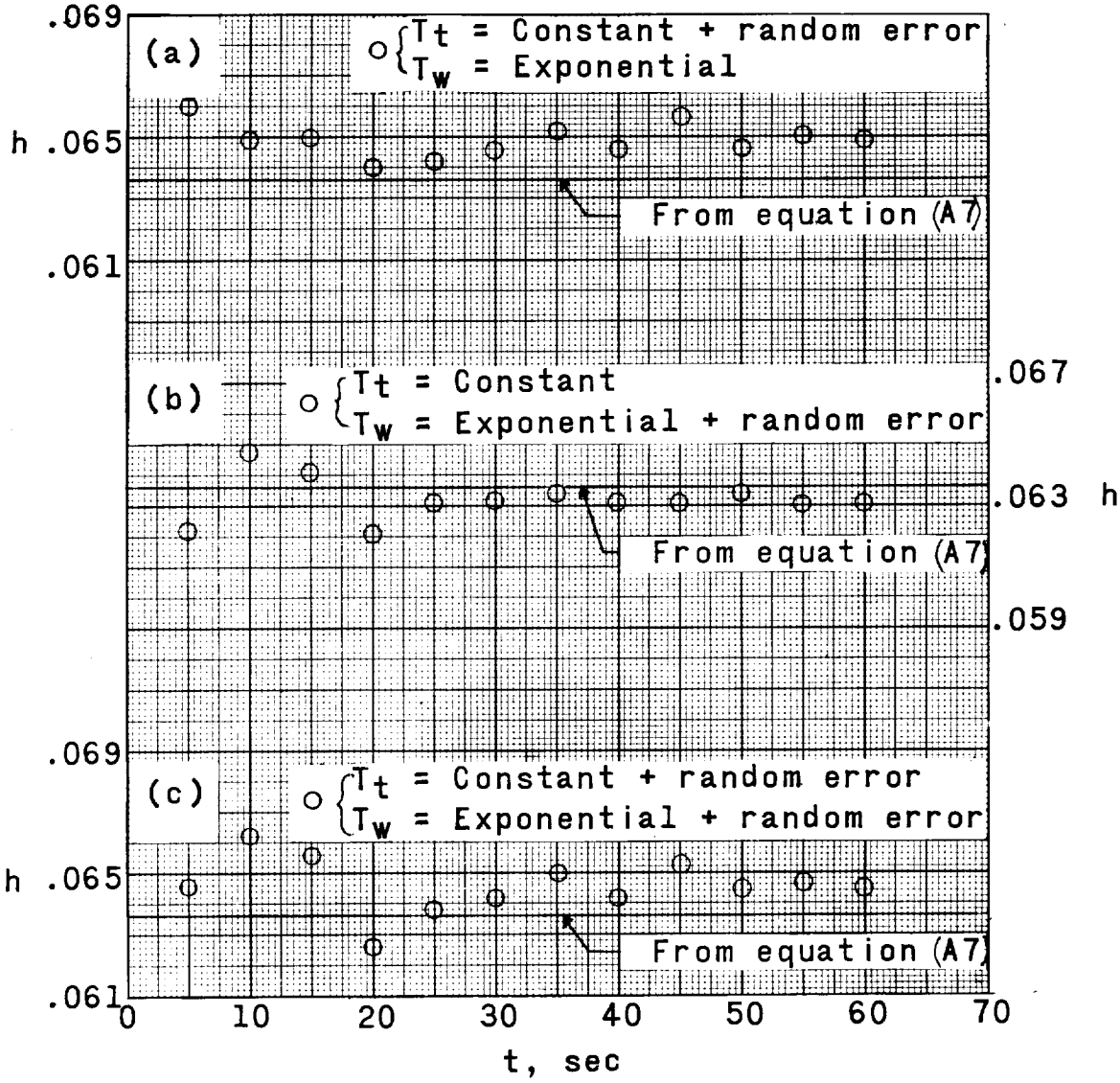

Figure 11.- Comparison of integral-solution heat-transfer coefficients on the 10° cone with theoretical values.

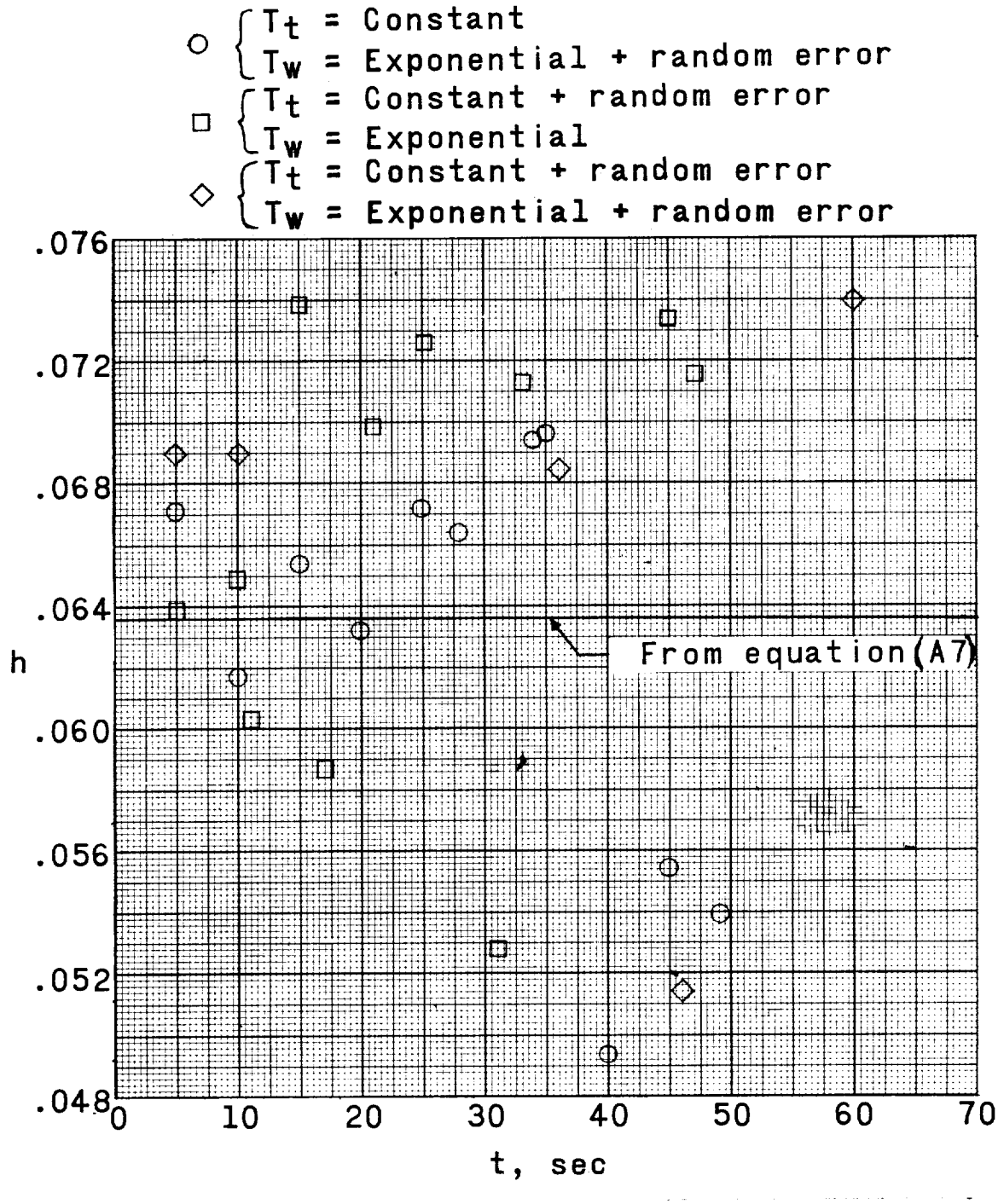

Figure 12.- Comparison of machine-slope heat-transfer coefficients on the 10° cone with theoretical values.

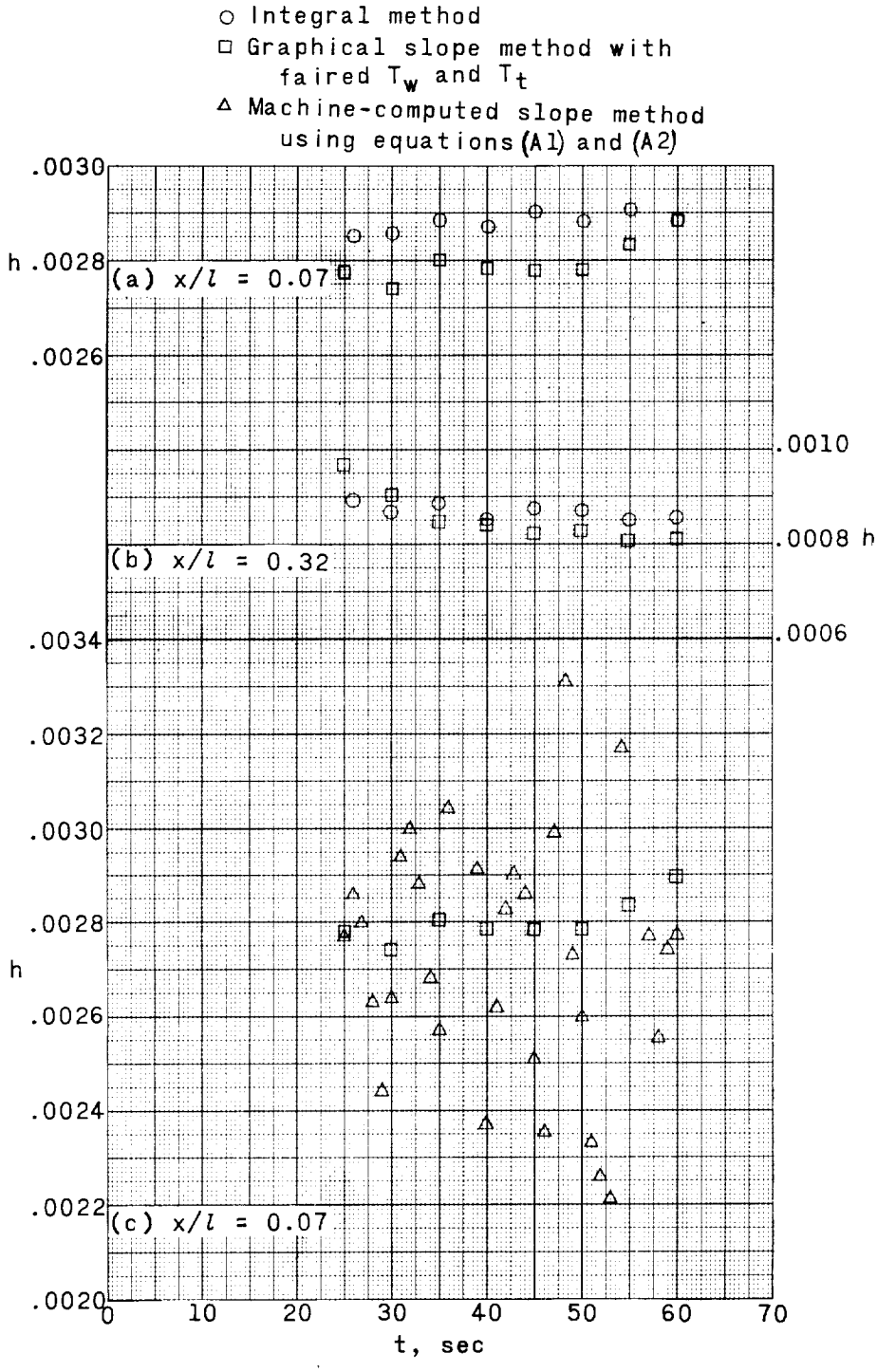

Figure 13.- Comparison of various methods for calculating the heat-transfer coefficients on the 10° cone.

NASA MEMO 6-4-59L
National Aeronautics and Space Administration.
DISTRIBUTION OF HEAT TRANSFER ON A 10° CONE AT ANGLES OF ATTACK FROM 0° TO 15° FOR MACH NUMBERS OF 2.49 TO 4.65 AND A SOLUTION TO THE HEAT-TRANSFER EQUATION THAT PERMITS COMPLETE MACHINE CALCULATIONS.
Paige B. Burbank and B. Leon Hodge. June 1959.
45p. diagrs., photo., tabs.
(NASA MEMORANDUM 6-4-59L)

The measured laminar heat-transfer coefficients at an angle of attack of 0° are in good agreement with Van Driest theory having a Mangler transformation. At angle of attack the heat-transfer coefficients along the stagnation line are 1.9 to 4 times greater than at an angle of attack of 0° depending upon the distance from the tip of the nose, Reynolds number, and Mach number. Boundary-layer transition and body vortices cause minimum heat-transfer coefficients to occur at the 90° and 120° meridian angles and increased aerodynamic heating along the 180° meridian that in some

Copies obtainable from NASA, Washington (over)

1. Flow, Laminar (1.1.3.1)
2. Flow, Turbulent (1.1.3.2)
3. Heat Transfer, Aerodynamic (1.1.4.2)

I. Burbank, Paige B.
II. Hodge, B. Leon
III. NASA MEMO 6-4-59L

NASA

NASA MEMO 6-4-59L
National Aeronautics and Space Administration.
DISTRIBUTION OF HEAT TRANSFER ON A 10° CONE AT ANGLES OF ATTACK FROM 0° TO 15° FOR MACH NUMBERS OF 2.49 TO 4.65 AND A SOLUTION TO THE HEAT-TRANSFER EQUATION THAT PERMITS COMPLETE MACHINE CALCULATIONS.
Paige B. Burbank and B. Leon Hodge. June 1959.
45p. diagrs., photo., tabs.
(NASA MEMORANDUM 6-4-59L)

The measured laminar heat-transfer coefficients at an angle of attack of 0° are in good agreement with Van Driest theory having a Mangler transformation. At angle of attack the heat-transfer coefficients along the stagnation line are 1.9 to 4 times greater than at an angle of attack of 0° depending upon the distance from the tip of the nose, Reynolds number, and Mach number. Boundary-layer transition and body vortices cause minimum heat-transfer coefficients to occur at the 90° and 120° meridian angles and increased aerodynamic heating along the 180° meridian that in some

Copies obtainable from NASA, Washington (over)

1. Flow, Laminar (1.1.3.1)
2. Flow, Turbulent (1.1.3.2)
3. Heat Transfer, Aerodynamic (1.1.4.2)

I. Burbank, Paige B.
II. Hodge, B. Leon
III. NASA MEMO 6-4-59L

NASA

NASA MEMO 6-4-59L
National Aeronautics and Space Administration.
DISTRIBUTION OF HEAT TRANSFER ON A 10° CONE AT ANGLES OF ATTACK FROM 0° TO 15° FOR MACH NUMBERS OF 2.49 TO 4.65 AND A SOLUTION TO THE HEAT-TRANSFER EQUATION THAT PERMITS COMPLETE MACHINE CALCULATIONS.
Paige B. Burbank and B. Leon Hodge. June 1959.
45p. diagrs., photo., tabs.
(NASA MEMORANDUM 6-4-59L)

The measured laminar heat-transfer coefficients at an angle of attack of 0° are in good agreement with Van Driest theory having a Mangler transformation. At angle of attack the heat-transfer coefficients along the stagnation line are 1.9 to 4 times greater than at an angle of attack of 0° depending upon the distance from the tip of the nose, Reynolds number, and Mach number. Boundary-layer transition and body vortices cause minimum heat-transfer coefficients to occur at the 90° and 120° meridian angles and increased aerodynamic heating along the 180° meridian that in some

Copies obtainable from NASA, Washington (over)

1. Flow, Laminar (1.1.3.1)
2. Flow, Turbulent (1.1.3.2)
3. Heat Transfer, Aerodynamic (1.1.4.2)

I. Burbank, Paige B.
II. Hodge, B. Leon
III. NASA MEMO 6-4-59L

NASA

NASA MEMO 6-4-59L
National Aeronautics and Space Administration.
DISTRIBUTION OF HEAT TRANSFER ON A 10° CONE AT ANGLES OF ATTACK FROM 0° TO 15° FOR MACH NUMBERS OF 2.49 TO 4.65 AND A SOLUTION TO THE HEAT-TRANSFER EQUATION THAT PERMITS COMPLETE MACHINE CALCULATIONS.
Paige B. Burbank and B. Leon Hodge. June 1959.
45p. diagrs., photo., tabs.
(NASA MEMORANDUM 6-4-59L)

The measured laminar heat-transfer coefficients at an angle of attack of 0° are in good agreement with Van Driest theory having a Mangler transformation. At angle of attack the heat-transfer coefficients along the stagnation line are 1.9 to 4 times greater than at an angle of attack of 0° depending upon the distance from the tip of the nose, Reynolds number, and Mach number. Boundary-layer transition and body vortices cause minimum heat-transfer coefficients to occur at the 90° and 120° meridian angles and increased aerodynamic heating along the 180° meridian that in some

Copies obtainable from NASA, Washington (over)

1. Flow, Laminar (1.1.3.1)
2. Flow, Turbulent (1.1.3.2)
3. Heat Transfer, Aerodynamic (1.1.4.2)

I. Burbank, Paige B.
II. Hodge, B. Leon
III. NASA MEMO 6-4-59L

NASA

NASA MEMO 6-4-59L

cases is of the same magnitude as along the zero meridian (stagnation line). A method was developed for complete machine calculation of the heat-transfer coefficient from transient temperature measurements.

Copies obtainable from NASA, Washington

NASA

NASA MEMO 6-4-59L

cases is of the same magnitude as along the zero meridian (stagnation line). A method was developed for complete machine calculation of the heat-transfer coefficient from transient temperature measurements.

Copies obtainable from NASA, Washington

NASA

NASA MEMO 6-4-59L

cases is of the same magnitude as along the zero meridian (stagnation line). A method was developed for complete machine calculation of the heat-transfer coefficient from transient temperature measurements.

Copies obtainable from NASA, Washington

NASA

NASA MEMO 6-4-59L

cases is of the same magnitude as along the zero meridian (stagnation line). A method was developed for complete machine calculation of the heat-transfer coefficient from transient temperature measurements.

Copies obtainable from NASA, Washington

NASA